船体まわり自由表面流れの計算法に関する研究

(59460130)

昭和61年度科学研究費補助金(一般研究Ｂ)研究成果報告書

昭和６２年３月

研究代表者　丸　尾　孟
(横浜国立大学工学部教授)

はしがき

本研究は昭和５９年４月より昭和６２年３月に至る３個年間にわたって，文部省科学研究費（一般研究Ｂ）の補助により行われたものである。

研究課題は一様な速度で前進する船体のまわりの自由表面を有する流れの理論解析に関するものである。従来この問題は１８９８年Ｊ.Ｈ.Ｍｉｃｈｅｌｌによって立てられた理論が中心となって解析されて来た。しかしながらこの理論を用いて計算した結果は実際の現象とはかなり差がある。実際に現象に合致する結果を与えるような理論を工夫することは多くの人々によって試みられて来たが，未だに実用に堪える成果を収めるには至っていない。今回の研究ではこれまで予備的な計算によってその有効性が期待出来る二つの方法によって具体的計算を遂行し，実測結果と比較してその実用性を実証せんとするものである。さらに近年とみに注目を集めつつある船首まわりの流れの理論的解明をも試みている。

研　究　組　織

研　究　代　表　者：丸　尾　　孟（横浜国立大学工学部・教授）

研　究　分　担　者：池　畑　光　尚（横浜国立大学工学部・教授）

鈴　木　和　夫（横浜国立大学工学部・助教授）

田草川　善　助（横浜国立大学工学部・助手）

研　究　経　費

昭和５９年度	３０００千円
昭和６０年度	２４００千円
昭和６１年度	１０００千円
計	６４００千円

研　究　発　表

(1) 学　会　誌　等

1) 荻原誠功・丸尾　孟

船体まわりの自由表面流れの非線形計算法，日本造船学会論文集，第１５７号
昭和６０年６月

2) H.Maruo・S.Ogiwara

A Method of Computation for Steady Ship-Waves with Non-linear Free Surface Conditions,Proceedings of Fourth International Conference on Numerical Ship Hydrodynamics. Sept.1985

3) 丸尾　孟

模型船首まわりの自由表面流れについて，日本造船学会論文集　第１５８号
昭和６０年１２月

4) H.Maruo・M.Ikehata

Some Discussions on the Free Surface Flow Around the Bow, Proceedings of Sixteenth Symposum on Naval Hydrodynamics, July 1986

(2) 口　頭　発　表

1) 丸尾　孟・石　仲堃・吉田　仁

没水円柱の運動による水面変形の非線形的計算，第３４回応用力学連合講演会
昭和５９年１２月１１日～１２日

2) H.Maruo

A Contribution to the Slender Body Theory in Ship Hydrodynamics, 14th International Congress of Theoretical and Applied Mechanics, 19-25 August 1984

3) H。Maruo

Effect of Surface Tension on the Free Surface Flow Around Floating Bodies in Motion, IUTAM Symposium on Fluid Mechanics in the Spirit of G.I。Taylor. 24-28 March 1986

研究成果の概要

本研究の内容は次のような3つの課題に分類することが出来る。

1) 細長体理論を船体まわりの自由表面流れに適用し，自由表面形状，船体表面流線，圧力分布，造波抵抗等の計算を行う。

2) 船体まわりの自由表面上の非線形境界条件を満足する解を，境界要素法の繰り返し計算によって数値的に求め，自由表面形状，船体表面圧力分布，造波抵抗の計算を行う。

3) 模型船の船首付近の自由表面現象について，特に表面張力の影響に着目して実験観察を行い，理論を用いてこの現象を解明する。

課題 1) については昭和58年度までに予備的研究が行われており、理論式の展開等はほぼ完成しているが，数値計算法についていくつかの問題点が残されていた。今回の研究ではこれらの問題点を解決し，さらに実用を目的とした計算に便利なプログラムの開発を行った。またこれまでに取り上げられていなかった斜航する船体に関する計算も行い，水面上の波紋，横方向の力およびモーメントの計算も行った。しかし得られた結果は精度の面で不充分な点が多いことが見出されたので，さらに精度の高い計算法の開発を行ったが，最終結果を得るには至っていない。

課題 2) については肥大船のまわりの自由表面流れの計算法として考案された低速理論を出発点として，自由表面条件の非線形項を取り入れた境界値問題を繰り返し計算によって解く方法を開発した。簡単な数式で表示される船型および，Series−60船型について，自由表面形状，圧力分布，造波抵抗を計算し，水槽実験と比較した結果は良好な一致を示し，肥大船を含む実用船型の造波抵抗計算法として実用性が確認された。

課題 3) については界面活性剤を用いて表面張力を除去して水槽試験を行うことにより，模型船首まわりの自由表面現象は表面張力によって顕著な影響を受けることが確認された。また模型船の抵抗は前進速度が約1.0 m/sec以下において，表面張力が作用する時と作用しない時とで異ることが示された。さらに表面張力を考慮して水面の波紋を理論解析し，相似則について検討を加えた。

研究成果

A Contribution to the Slender Body Theory in Ship Hydrodynamics

by Hajime Maruo (Lecture)

Yokohama National Universiy

156 Tokiwadai Hodogaya-ku Yokohama Japan

Abstract:

The application of the slender body theory to ship hydrodynamics was proposed more than twenty years ago. In spite of the remarkable success of the slender body theory in aerodynamics, it has been revealed that the formulation in ship hydrodynamics proposed so far yields only disappointing results by numerical computation. Though some improvement has been observed in the problem of oscillating ships in waves, progress in the problem of steady forward motion is rather poor.

In this paper, a new formulation of the slender body theory for a ship with constant forward speed is developed. It is based on a suitable asymptotic expansion of the Kelvin source along its track. It derives a boundary value problem which has a quite different form from that of the formulation proposed before. Sample computations of the ship wave pattern and wave resistance show good agreement with measured results.

It is concluded that the present theory is feasible as a prediction method of ship waves and wave resistance of arbitrary hull forms.

transparency 6

COMPARISON OF THEORETICAL AND MEASURED WAVE PATTERN OF SERIES 60, C_B=0.60 AT F_n= 0.304

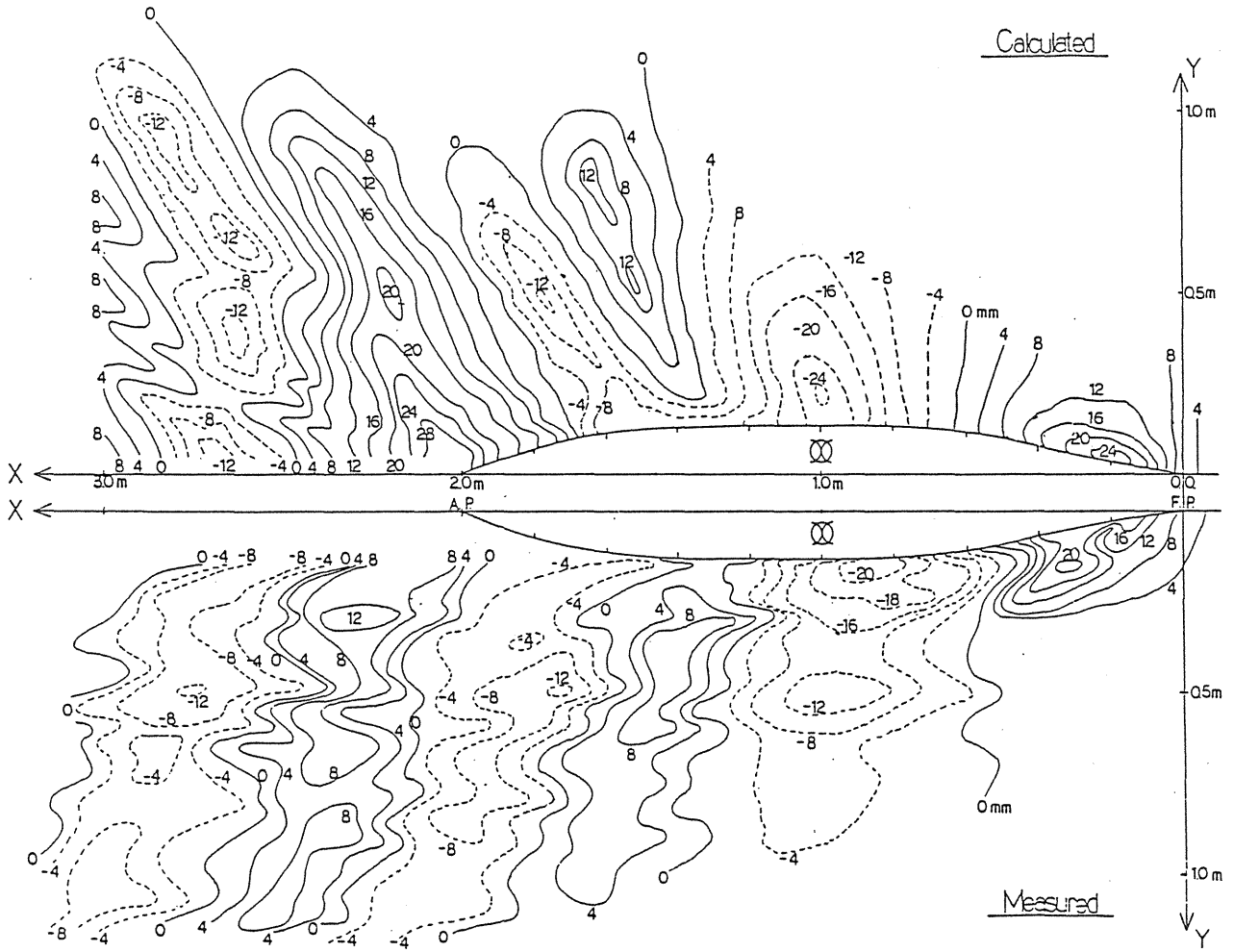

transparency 7

COMPARISON OF COMPUTED AND MEASURED WAVE PROFILES AT $F_n = 0.304$

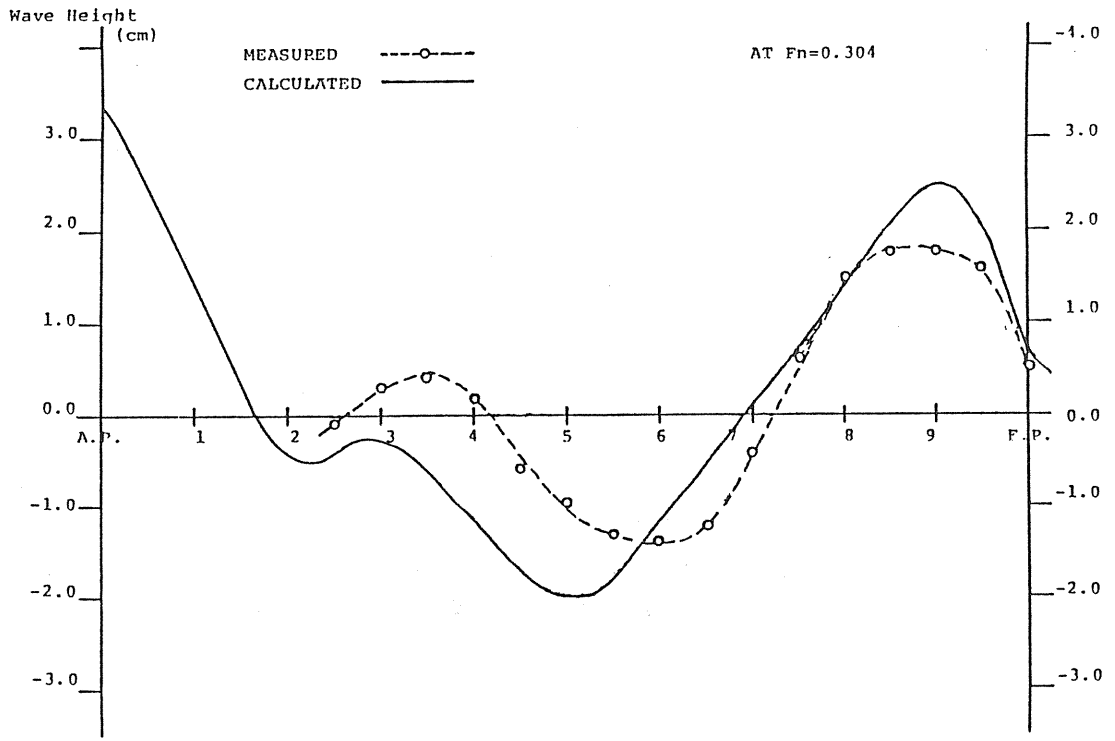

WAVE RESISTANCE COEFFICIENT OF SERIES 60. $C_B = 0.6$

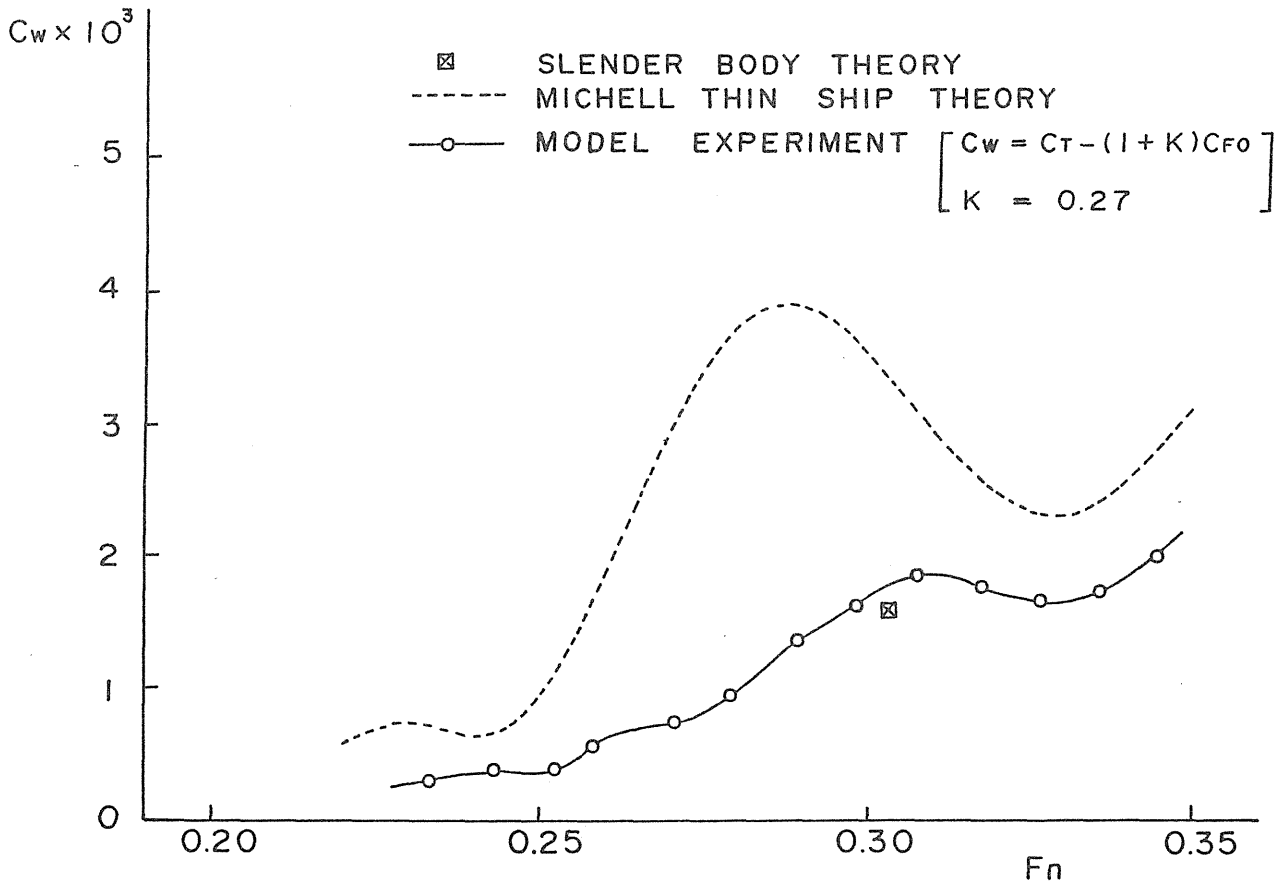

以下の頁は著作権者の許諾を得ていないため、公表できません。

p. 9 ~ p. 21

p. 34 ~ p. 42

p. ~ p.

p. ~ p.

p. ~ p.

A Method of Computation for Steady Ship-Waves with Non-linear Free Surface Conditions

Hajime Maruo
Yokohama Natinal University, Yokohama

Seikoo Ogiwara
Ishikawajima-Harima Heavy Industries, Yokohama

1. Introduction

The theory of ship waves is a substantially non-linear problem. The method which has been commonly used in order to solve this problem is the perturbation analysis with the assumption of small beam/length ratio of the ship. The Michell thin ship theory is the first approximation of the perturbation and a great number of examples of wave resistance computation has been published so far. Tsutsumi et al.(1) compared the wave resistance determined by the wave pattern analysis of mathematically defined ship model of variable breadth with corresponding computations by Michell's formula, and concluded that Michell's formula could predict the wave resistance within the torelable accuracy in case of beam/length ratio not greater than one fifteenth.

Since practical hull forms exceed this limitation, Michell's formula is not useful for the purpose of prediction of wave resistance. The higher approximation of the thin ship perturbation has been attempted by several researchers(2)(3)(4), but the results are not so promising, because of the highly singular behavior of the Kelvin source which prevents the feasibility of the higher approximation.

Another possibility of the perturbation analysis is the low Froude number approach. This method assumes the series expansion of the solution with respect to the Froude number. The starting point is the flow at zero Froude number which is identical with the flow around a double model in an unbounded fluid. The free surface condition for the disturbance potential is then linearized and the solution is simplified to a great extent. This idea was firstly suggested by Ogilvie(5) for the motion in two-dimensions, and applications to the three-dimensional case have been discussed by Baba et al.(6) and Maruo et al(7). Dawson(8) proposed a purely numerical method to solve the boundary value problem with the free surface condition similar to the above approximation by the aid of the distribution of Rankine sources over the still water plane together with the hull surface. A computer program for this method applicable to arbitrary hull forms was developod by Ogiwara(9) who calculated the wave profile, pressure distribution on the hull surface and the wave resistance and examined the feasibility of this method in the practical field.

Apart from the technique of linearized free surface conditions, the possibility of the direct solution of the boundary value problem in its original non-linear form depends only on numerical methods. A typical method of this kind is the finite difference technique, by which the solution is obtained by the step by step integration of the unsteady Euler or Navier-Stokes equation with respect to time. Several results of computation by the finite difference technique applied to hull forms have been published by Chan et al.(10) and Aoki et al.(11). Serious disadvantages of this method are that an enormous computer time is required before the steady state is finally attained and that a proper treatment of the condition at the open boundary with which the domain of computation is encompassed is hardly possible. On account of these defects, it is quite unlikely for the accuracy of computation by this method to be able to attain the level of practical feasibility.

The method proposed here is a kind of the boundary element method with the Rankine source as the kernel function. The steady non-linear free surface flow around a hull placed in a uniform stream is determined by iteration so as to fulfil the non-linear free surface condition and the hull surface condition, starting from the solution of double model linearization such as Dawson's problem. An advantage of this method is that the computer program for the double model linearization ,which is now at hand, is fully utilized. Other points of merit is that an analytical expression can be given to the solution at the final stage by means of the source distribution over the boundary and that the condition at infinite depth is fulfiled automatically. It has been found on carrying out the computation, that the stability in computation process is a serious problem, and several techniques to suppress the instability are indispenable. In order to examine problems associated to numerical technique, computations are executed for the two-dimensional motion of a submerged cylinder(12). Then numerical examples of three dimensional calculation are shown with respect to the wave pattern, pressure distribution and wave resistance of mathematically defined hull forms(13).

2. Basic formulation

Take cartesian coordinates with axes of x and y in the undisturbed free surface, and z axis in the vertically upward direction. Consider a ship hull fixed in a uniform flow of velocity U in the direction of x axis and assume an irrotational motion of an inviscid and incompressible fluid around the hull. The flow field is then defined by a velocity potential ϕ which satisfied the Laplace equation in the domain occupied by the fluid.

$$\phi_{xx}+\phi_{yy}+\phi_{zz}=0 \tag{1}$$

where subscripts mean partial derivatives. Designate the free surface elevation by the equation

$$z=\zeta(x,y) \tag{2}$$

and the boundary conditions on the free surface are as follows.

kinematical condition
$$\phi_x\zeta_x+\phi_y\zeta_y-\phi_z=0 \quad (z=\zeta) \tag{3}$$

dynamical condition
$$\frac{1}{2}(\phi_x^2+\phi_y^2+\phi_z^2-U^2)+g\zeta=0 \quad (z=\zeta) \tag{4}$$

where g is the acceleration of gravity. There is a condition at infinity such as $\phi=Ux$ at $x^2+y^2+z^2=\infty$. We have to consider generally the radiation condition that there is no wave motion at infinite upstream, but results of computations have shown that this condition is fulfiled by adoption a suitable computation algorithm. The free surface conditions, (3) and (4), have to be satisfied on the elevated free surface $z=\zeta(x,y)$, but trial computation has shown that the adoption of values at the real free surface at each step of iteration causes an unavoidable tendency of divergence. Therefore we employ an approximation that each value at $z=\zeta$ is expanded in Taylor series around z=0 and higher order terms are omitted. Resulting equations are

$$\begin{aligned}&\phi_x\zeta_x+\phi_y\zeta_y-\phi_z-\phi_{zz}\zeta\\&=\phi_x\zeta_x+\phi_y\zeta_y-\phi_z+(\phi_{xx}+\phi_{yy})\zeta=0 \quad (z=0)\end{aligned} \tag{5}$$

$$\begin{aligned}&\frac{1}{2}(\phi_x^2+\phi_y^2+\phi_z^2-U^2)\\&+\{\phi_x\phi_{zx}+\phi_y\phi_{zy}-\phi_z(\phi_{xx}+\phi_{yy})\}\zeta\\&+g\zeta=0 \quad (z=0)\end{aligned} \tag{6}$$

These equations are satisfied on the plane z=0.

The method of solution is based on the decomposition of the velocity potential into the double model flow potential ϕ_0 and the deviation from it such as

$$\phi=\phi_0+\phi_1 \tag{7}$$

The double model potential is regarded as a known function. Substituting (7) in (5) and (6), one obtains after some reduction

$$\begin{aligned}&\phi_{0x}\zeta_x+\phi_{1x}\zeta_{0x}+\phi_{0y}\zeta_y+\phi_{1y}\zeta_{0y}\\&-\phi_{1z}+D_1(x,y)=0 \quad (z=0)\end{aligned} \tag{8}$$

$$\begin{aligned}\zeta=&\frac{1}{2g}(U^2-\phi_{0x}^2-\phi_{0y}^2-2\phi_{0x}\phi_{1x}-2\phi_{0y}\phi_{1y})\\&+D_2(x,y) \quad (z=0)\end{aligned} \tag{9}$$

where

$$\zeta_0=\frac{1}{2g}(U^2-\phi_{0x}^2-\phi_{0y}^2) \tag{10}$$

$$\begin{aligned}D_1(x,y)=&\phi_{1x}(\zeta_x-\zeta_{0x})+\phi_{1y}(\zeta_y-\zeta_{0y})\\&+(\phi_{0xx}+\phi_{0yy}+\phi_{1xx}+\phi_{1yy})\zeta\end{aligned} \tag{11}$$

$$\begin{aligned}D_2(x,y)=&-\frac{1}{2g}(\phi_{1x}^2+\phi_{1y}^2+\phi_{1z}^2)\\&-\frac{1}{g}\{(\phi_{0x}+\phi_{1x})\phi_{1xx}+(\phi_{0y}+\phi_{1y})\phi_{1xy}\\&-\phi_{1z}(\phi_{0xx}+\phi_{0yy}+\phi_{1xx}+\phi_{1yy})\}\zeta\end{aligned} \tag{12}$$

$D_1(x,y)$ and $D_2(x,y)$ indicate the non-linear effect. If we omit the non-linear terms, i.e. $D_1(x,y)=0$, $D_2(x,y)=0$ we have the boundary condition for the double model linearized solution.

$$\begin{aligned}&\frac{1}{2}\{\phi_{0x}(\phi_{0x}^2+\phi_{0y}^2)_x+\phi_{0y}(\phi_{0x}^2+\phi_{0y}^2)_y\}\\&+\{\phi_{0x}(\phi_{0x}\phi_{1x}+\phi_{0y}\phi_{1y})_x\\&+\phi_{0y}(\phi_{0x}\phi_{1x}+\phi_{0y}\phi_{1y})_y\}\\&+\frac{1}{2}\{\phi_{1x}(\phi_{0x}^2+\phi_{0y}^2)_x+\phi_{1y}(\phi_{0x}^2+\phi_{0y}^2)_y\}\\&+g\phi_{1z}=0 \quad (z=0)\end{aligned} \tag{13}$$

If we take the length s along the streamline on the plane z=0 of the double model flow, the above equation can be transformed into

$$\phi_{0s}^2\phi_{1ss}+2\phi_{0s}\phi_{0ss}\phi_{1s}+g\phi_{1z}=-\phi_{0s}^2\phi_{0ss} \quad (z=0) \tag{14}$$

This equation is identical with the double model linearized free surface condition which was employed by Dawson.

The boundary condition on the hull surface is the usual form

$$\frac{\partial\phi}{\partial n}=\frac{\partial\phi_0}{\partial n}+\frac{\partial\phi_1}{\partial n}=0 \tag{15}$$

where n is taken along the outward normal of the hull surface. Since the double model flow satisfies the hull surface condition, i.e. $\partial\phi_1/\partial n=0$, the boundary condition for ϕ_1 becomes

$$\frac{\partial\phi_1}{\partial n}=\phi_{1x}n_x+\phi_{1y}n_y+\phi_{1z}n_z=0 \tag{16}$$

where n_x, n_y, n_z are direction cosines of the normal.

We express the double model potential by a distribution of sources over the double hull surface such as

$$\phi_0(x,y,z)=Ux-\iint_{S_0}\sigma_0\left(\frac{1}{r_0}+\frac{1}{\bar{r}_0}\right)ds \tag{17}$$

where

$$r_0=\sqrt{(x-x')^2+(y-y')^2+(z-z')^2}$$
$$\bar{r}_0=\sqrt{(x-x')^2+(y-y')^2+(z+z')^2}$$

The velocity potential ϕ_1, on the other hand, is expressed by sources distributed on the hull surface S_0 and still water plane outside the hull S_1 as follows.

$$\phi_1(x,y,z)=-\iint_{S_0}\Delta\sigma_0\left(\frac{1}{r_0}+\frac{1}{\bar{r}_0}\right)ds-\iint_{S_1}\sigma_1\frac{1}{r_1}ds \tag{18}$$

where

$$r_1=\sqrt{(x-x')^2+(y-y')^2+z^2}$$

Now the boundary value problem is stated in such a manner that the source distribution densities σ_1, $\Delta\sigma_0$ are to be determined so as to make the velocity potentials ϕ_0 and ϕ_1 satisfy the boundary conditions (8),(9) and (16).

3. The numerical method of solution

The method of solution is an iterative procedure that the free surface conditions (8) and (9) are satisfied by assuming the non-linear terms $D_1(x,y)$and $D_2(x,y)$ are given by the solution of preceding step of iteration. In the first place, the double model source distribution σ_0 in (17) is determined in such a way that the hull boundary condition.

$$\frac{\partial\phi_0}{\partial n}=0 \tag{19}$$

is satisfied. Then the first approximation is obtained by determining the source densities $\Delta\sigma_0$ and σ_1 in (18) so as to satisfy the double model linearized free surface condition (14) together with the hull boundary condition (16). Next the functions $D_1(x,y)$, and $D_2(x,y)$ are calculated making use of the first approximation for ϕ_1. The first approximation for the free surface elevation is determined by substitution of ϕ_1 in (9) by the first approximation obtained above. The second approximation for the source densities $\Delta\sigma_0$ and σ_1 in (18) is determined so as to satisfy the hull boundary condition (16) and the free surface condition (8) in which $D_1(x,y)$ is determined by the first approximation. A similar process is repeated in further approximation.

The computation program, which has been developed for the solution of double model linearization, is effectively utilized in this iterative solution. It is found by a sample calculation, that inherent instability results divergence in repeated computation. In oder to eliminate this instability, a relaxation factor $\alpha_1<1.$ is mutiplied to the non-linear terms $D_1(x,y)$and $D_2(x,y)$.

The numerical work is carried out with discretization of the boundary surfaces. We make the hull surface S_0 consist of M_0 panels and take a finite area S_1 on the plane $z=0$, which is divided into M_1 elements, as the domain of computation. If the density of source is constant in one panel, velocity of the disturbance potential ϕ_1 are given by

$$\begin{aligned}\phi_{1x}&=\sum_{j=1}^{M_0}\Delta\sigma_0(j)CX_0(ij)+\sum_{j=1}^{M_1}\sigma_1(j)CX_1(ij)\\ \phi_{1y}&=\sum_{j=1}^{M_0}\Delta\sigma_0(j)CY_0(ij)+\sum_{j=1}^{M_1}\sigma_1(j)CY_1(ij)\\ \phi_{1z}&=\sum_{j=1}^{M_0}\Delta\sigma_0(j)CZ_0(ij)+\sum_{j=1}^{M_1}\sigma_1(j)CZ_1(ij)\end{aligned} \tag{20}$$

where (CX_0, CY_0, CZ_0) and (CX_1, CY_1, CZ_1) are velocities due to unit sources distributing on each panel and are given by

$$\begin{aligned}CX_0(ij)&=\iint_{S_{0j}}(x_i-x_j)\left(\frac{1}{r_{0ij}^3}+\frac{1}{\bar{r}_{0ij}^3}\right)ds\\ CY_0(ij)&=\iint_{S_{0j}}(y_i-y_j)\left(\frac{1}{r_{0ij}^3}+\frac{1}{\bar{r}_{0ij}^3}\right)ds\\ CZ_0(ij)&=\iint_{S_{0j}}\left(\frac{z_i-z_j}{r_{0ij}^3}+\frac{z_i+z_j}{\bar{r}_{0ij}^3}\right)ds\\ CX_1(ij)&=\iint_{S_{1j}}\frac{x_i-x_j}{r_{1ij}^3}ds\\ CY_1(ij)&=\iint_{S_{1j}}\frac{y_i-y_j}{r_{1ij}^3}ds\\ CZ_1(ij)&=\iint_{S_{1j}}\frac{z_i}{r_{1ij}^3}ds\end{aligned} \tag{21}$$

Integrals are performed in each panel on the hull surface or on the still water plane.

Because of the application of the relaxation factor α_1, the free surface condition takes the form like

$$\phi_{0x}\zeta_x+\phi_{1x}\zeta_{0x}+\phi_{0y}\zeta_y+\phi_{1y}\zeta_{0y}-\phi_{1z}+\alpha_1\cdot D_1(x,y)=0 \tag{22}$$

$$\zeta=\frac{1}{2g}(U^2-\phi_{0x}^2-\phi_{0y}^2-2\phi_{0x}\phi_{1x}-2\phi_{0y}\phi_{1y})+\alpha_1\cdot D_2(x,y) \tag{23}$$

Substituting (11) in (22), one obtains

$$\phi_{1x}A_x+\phi_{1y}A_y+\alpha_1\cdot\zeta(\phi_{1xx}+\phi_{1yy})-\phi_{1z}=B \tag{24}$$

where

$$A_x=\zeta_{0x}+\alpha_1(\zeta_x-\zeta_{0x}) \tag{25}$$

$$A_y=\zeta_{0y}+\alpha_1(\zeta_y-\zeta_{0y}) \tag{26}$$

$$B=-\phi_{0x}\zeta_x-\phi_{0y}\zeta_y-\alpha_1\cdot\zeta(\phi_{0xx}+\phi_{0yy}) \tag{27}$$

The free surface elevation is calculated by (23),(12) as follows.

$$\zeta=\frac{1}{2}\frac{U^2-\phi_{0x}^2-\phi_{0y}^2-2\phi_{0x}\phi_{1x}-2\phi_{0y}\phi_{1y}-\alpha_1(\phi_{1x}^2+\phi_{1y}^2+\phi_{1z}^2)}{g+\alpha_1[\phi_x\phi_{1xz}+\phi_y\phi_{1zy}-\phi_{1z}(\phi_{xz}+\phi_{yy})]} \tag{28}$$

The boundary conditions on the free surface and on the hull surface are written in discretized forms like

$$\sum_{j=1}^{M_0}\Delta\sigma_0(j)A_0(ij)+\sum_{j=1}^{M_1}\sigma_1(j)A_1(ij)+2\pi\sigma_1(i)=B(i) \tag{29}$$

$$(i=1,2,\cdots,M_1 \text{ on } S_1)$$

$$\sum_{j=1}^{M_0}\Delta\sigma_0(j)N_0(ij)+\sum_{j=1}^{M_1}\sigma_1(j)N_1(ij)=0 \tag{30}$$

$$(i=1,2,\cdots,M_0 \text{ on } S_0)$$

where

$$A_m(ij)=CX_m(ij)n_x(i)+CY_m(ij)n_y(i)+\alpha_1\zeta(CXX_m+CYY_m) \tag{31}$$

$$B(i)=-\phi_{0x}(i)\zeta_x(i)-\phi_{0y}(i)\zeta_y(i)-\alpha_1\zeta(i)[\phi_{0xx}(i)+\phi_{0yy}(i)] \tag{32}$$

$$CXX_m=[CX_m(x=x_1)-CX_m(x=x_1-\Delta x)]/\Delta x$$
$$CYY_m=[CY_m(y=y_1)-CY_m(y=y_1-\Delta y)]/\Delta y \tag{33}$$

$$N_m(ij)=CX_m(ij)\cdot n_x(i)+CY_m(ij)\cdot n_y(i)+CZ_m(ij)\cdot n_z(i) \tag{34}$$
$$N_0(ii)=2\pi+n_z(i)\iint_{S_{0i}}\frac{ds}{4\pi r_1^2}$$

Subscript m=0 means the contribution of sources on the hull surface and m=1 means that on the still water plane. The equation (29) and (30) give a system of simultaneous equations which determine the source densities σ_1 and $\Delta\sigma_0$

4. A simplified method

The method of computation stated in the preceding section requires long computer time because the boundary conditions on the hull surface and those on the free surface should be satisfied simultaneously. This fact is a serious disadvantage in view of the practical application. A simplified method is proposed here under this circumstance. Assume the hull surface source $\Delta\sigma_0^{(k)}$ and free surface elevation $\zeta^{(k)}$ at k-th step to be given. Then the free surface source $\sigma_1^{(k+1)}$ at (k+1)-th step is determined by the equation

$$\sum_{j=1}^{M_1}\sigma_1(j)^{(k+1)}A(ij)+2\pi\sigma_1(i)^{(k+1)}=C(i)^{(k)} \tag{35}$$

$$(i=1,2,\cdots,M_1 \text{ on } S_1)$$

where

$$C(i)^{(k)}=B(i)-\sum_{j=1}^{M_0}\Delta\sigma_0(j)^{(k)}A_0(ij) \tag{36}$$

The source distribution thus obtained induces the normal velocity on the hull surface given by

$$v_n(i)=\sum_{j=1}^{M_1}[\sigma_1(j)^{(k+1)}-\sigma_1(j)^{(k)}]N_1(ij) \tag{37}$$

In order to compensate the above velocity, source of density

$$\varepsilon=-\frac{1}{4\pi}v_n(i) \tag{38}$$

are added to the hull surface sources. Then the source distribution on the hull surface is of the density $\Delta\sigma_0(i)+\varepsilon$. The computation begins with the first approximation which is obtained from the double-model-linearized solution with free surface condition (14). The first approximation for ζ is obtained from

$$\zeta(x,y)=\frac{1}{2g}(U^2-\phi_{0x}^2-\phi_{0y}^2-2\phi_{0x}\phi_{1x}-2\phi_{0y}\phi_{1y}) \tag{39}$$

The second approximation for the free surface source density σ_1 is determined by solving the simultaneous equations (35) and the hull surface source density is obtained from (37) and (38). The similar process is repeated in the further approximation untill a stationary value is obtained. It has been found during trial computations, that adjustment of interval between each step is needed during iteration in order to keep stability. Therefore another relaxation factor $\alpha_2<1$, by which ζ in the (k+1)-th step is modified such as

$$\bar{\zeta}(i)^{(k+1)}=\zeta(i)^{(k)}+\alpha_2[\zeta(i)^{(k+1)}-\zeta(i)^{(k)}] \tag{40}$$

The flow diagram of the numerical work is shown in Fig.1. The partial derivatives, which are necessary for the determination of coefficient in (35), are calculated by the following fashion.

Consider a function f(x,y) in x-y plane and define a plane given by the equation

$$ax+by+cf=1 \tag{41}$$

on which three point $(x_i, y_i, f_i,\ i=1,2,3)$ are located. Then the partial derivatives of f(x,y) are approximated by

$$f_x=-\frac{a}{c},\quad f_y=-\frac{b}{c} \tag{42}$$

A trial computation for the two-dimensional problem of a submerged elliptic cylinder shows that results obtained by the simplified method are sufficiently accurate when compared with the results by the more complicated method in the preceding section.

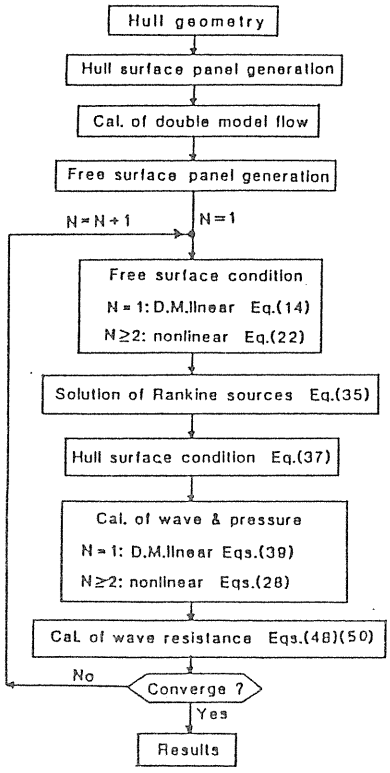

Fig.1 Flow diagram of numerical computation

5. The wave profile of a submerged elliptic cylinder

In oder to examine the validity of the computation method mentioned above, the method of section 3 is applied to the two-dimensional problem of the wave profile which accompany a submerged cylinder of elliptic section. The numerical example is concerning the shape with the ratio between two axes a/b=4.

Fig.2 shows the results of computation at each step of iteration for the case of $Fn=U/\sqrt{2ga}=0.5$, f/a=1.7 (f is the depth of immersion of the center) when the relaxation factor α_1, α_2 are not applied. Instability of computation is observed which make the result diverge at the 7th step. After some study, it is found that stable results are obtained by application of the relaxation factor $\alpha_1=0.75$, $\alpha_2=0.25$ as shown in Fig.3. The convergence of the computation is examined by the quantity

$$E(k)=\sum_{i=1}^{M_1}|\eta_{(i)}^{(k+1)}-\eta_{(i)}^{(k)}|^2 \qquad (43)$$

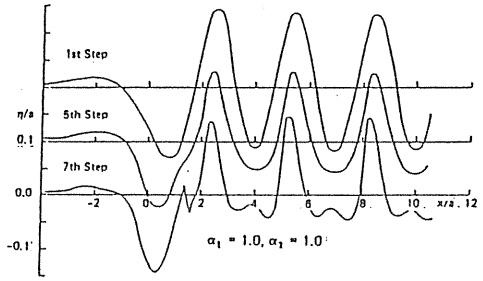

Fig.2 Wave profile at each step of iteration process (f/a=1.7, Fn=0.50, α_1=1.0, α_2=1.0)

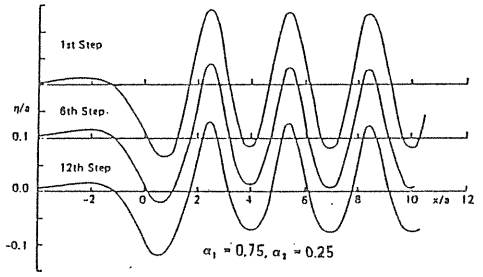

Fig.3 Wave Profile at each step of iteration process (f/a=1.7, Fn=0.50, α_1=0.75, α_2=0.25)

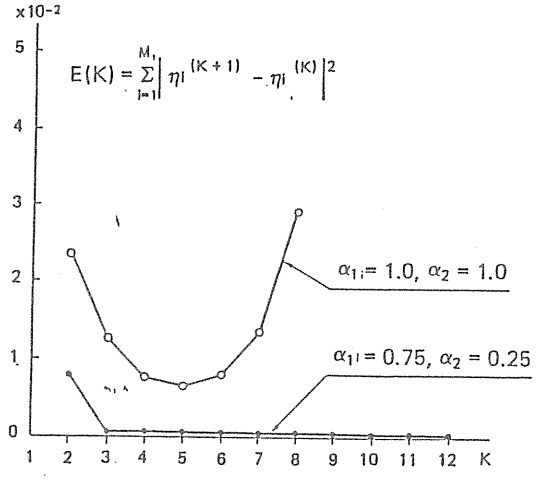

Fig.4 Convergence of wave profile (f/a=1.7, Fn=0.50)

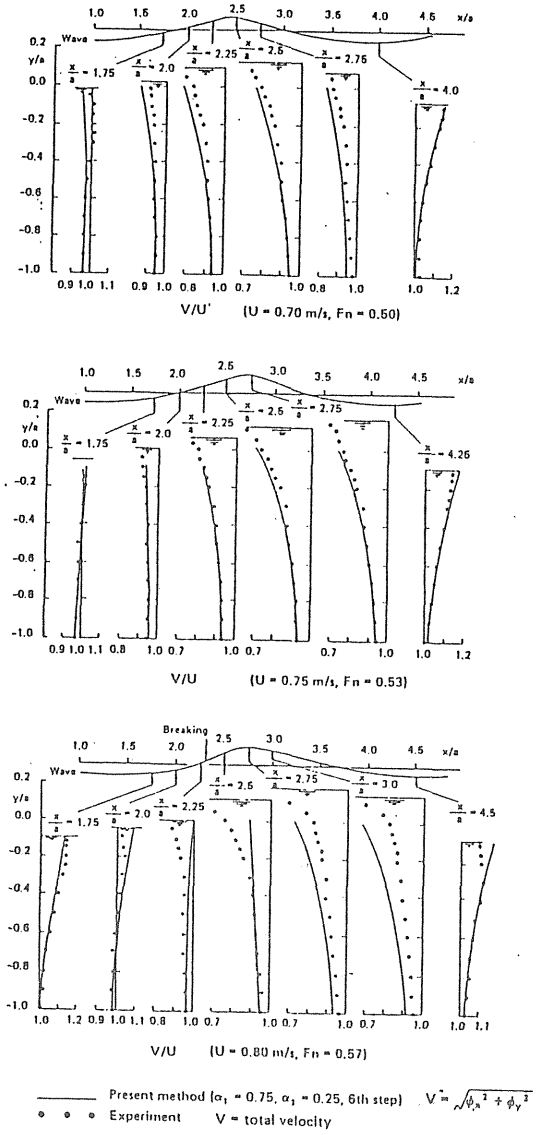

Fig.7 Comparison of velocity distribution beneath free surface (f/a=1.7)

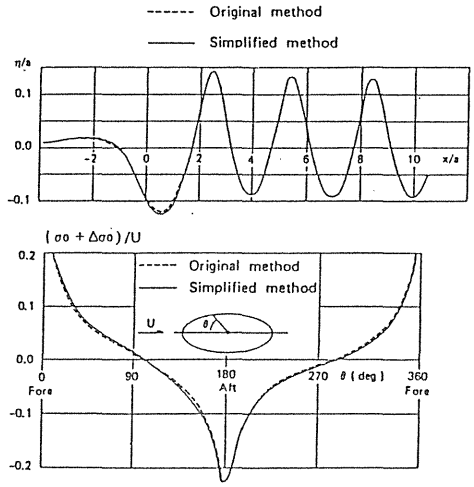

Fig.8 Comparison of wave profile (above) and source distribution on the ellipse(bellow) (Fn=0.50, f/a=1.7, α_1=0.75, α_2=0.25, 6th step)

This is a version of Wigley model, with fuller entrance. The panel division on the hull surface and on the still water plane is shown in Fig.9. The number of panels on the hull surface on one side is 27x10 and that on the still water plane is 44x9.

The effect of the relaxation factors is studied in the first place by computations with variable α_1 and α_2. Fig.10 gives the wave profiles with changing α_1 applied. The effect of variation in α_2 is shown in Fig.11. According to these results, stable iteration may be obtained by the adoption of α_1=0.50 and α_2=0.10, but instability still takes place at $Fn=U/\sqrt{gL}=0.267$ in this case. It is understood that the instability due to non-linearity appears in a limited zone near both ends of the hull, and the application of α_1 is needed only in the above zone. Therefore we apply the relaxation factor in two circular regions of radius $\lambda/2$ with centers at F.P. and A.P. of the hull as shown in Fig.12. Here λ is the wave length $\lambda=2\pi U^2/g$. The distribution of α_1 is given by

$$\alpha_1=\begin{cases}\alpha_B+2r(\alpha_A-\alpha_B)/\lambda & (0\leqq r\leqq\lambda/2)\\ \alpha_A & (r>\lambda/2)\end{cases} \qquad (46)$$

We employ α_A=1.0, α_B=0.25, α_2=0.1 in further computations. Fig.13 shows the results of computation at each step of iteration process. Change of value is significant at both ends of the hull. The results of computation are compared with measurements in the towing tank. Fig.14 shows the comparison of wave profile alongside the model (Model A), and Fig.15 shows the computed and measured pressure distribution at the level z/d=-0.52. Much better agreement with measured results is obtained by the present method than by the Michell thin ship theory.

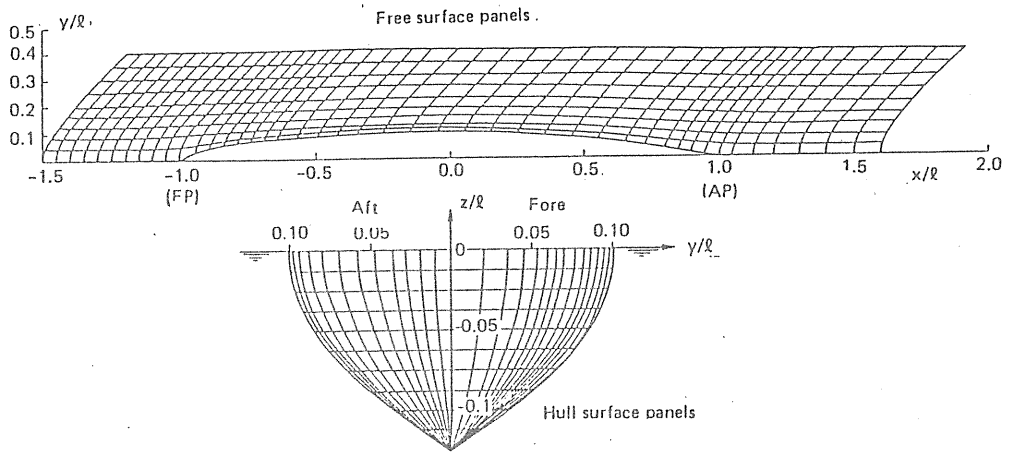

Fig.9 Panel division on the boundary surfaces for Model A

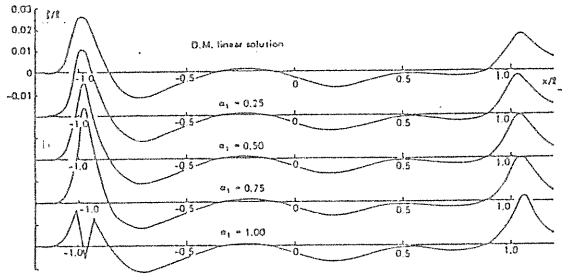

Fig.10 The effect of correction factor A1 on wave profile (Model A, Fn=0.250, α_2=0.10, 4th step)

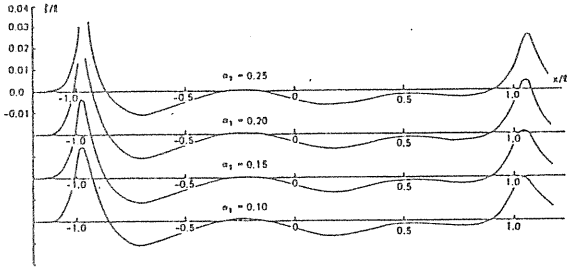

Fig.11 The effect of correction factor A2 on wave Profile (Model A, Fn=0.250, α_1=0.50, 4th step)

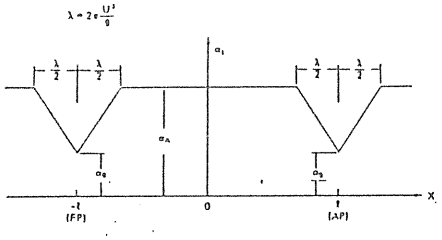

Fig.12 Distribution of correction factor

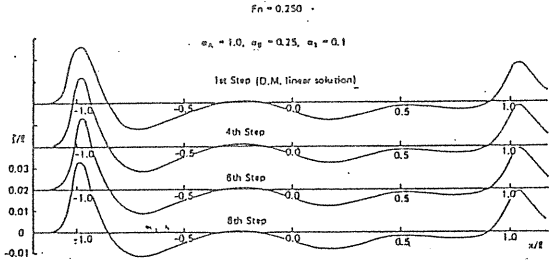

Fig.13 Wave profile at each step of iteration process (Model A)

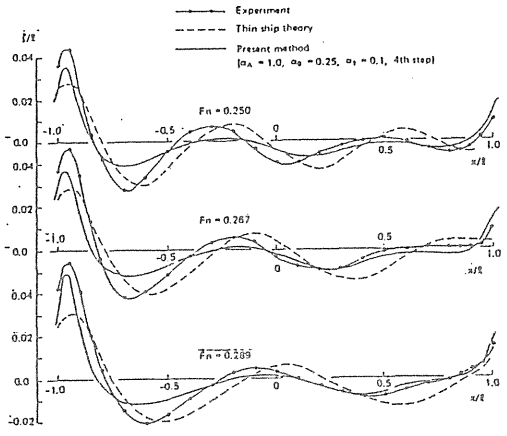

Fig.14 Comparison of wave profiles of Model A

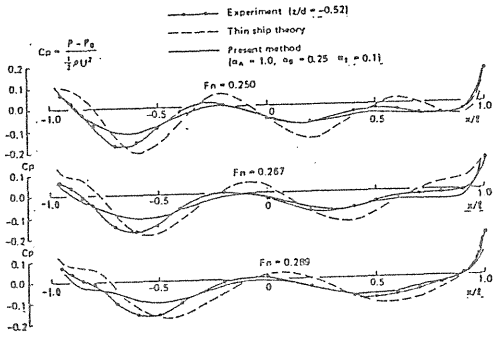

Fig.15 Comparison of pressure distribution for Model A at z/d=-0.52

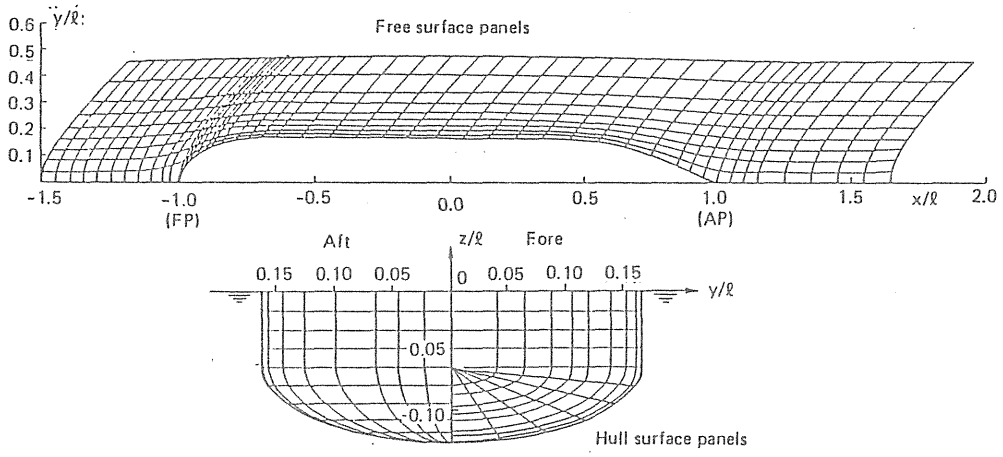

Fig.16 Panel division on the boundary surfaces for Model B

The second example is a much fuller model (Model B) with elliptic bow waterline and elliptic frame lines. The panel division for the numerical work is shown in Fig.16, and the mathematical expression for the hull surface is given in Table 1.

Fig.17 shows the comparison of the computed wave profile with the measurement and Fig.18 shows the pressure distribution at the level z/d=-0.3. Good agreement is observed in the fore-body, but there are some discrepancies in the aft-body. The difference between the computation and the measurement in the aft-body may be attributed to the viscosity effect. Fig.19 gives a schematical illustration of wave patterns of both models.

7. The wave resistance

The fluid pressure is given by Bernoulli's theorem such as

$$p-p_0=\frac{1}{2}\rho\{U^2-\phi_{0x}^2-\phi_{0y}^2-\phi_{0z}^2-2\phi_{0x}\phi_{1x} -2\phi_{0y}\phi_{1y}-2\phi_{0z}\phi_{1z} -\alpha_1(\phi_{1x}^2+\phi_{1y}^2+\phi_{1z}^2)\} \tag{47}$$

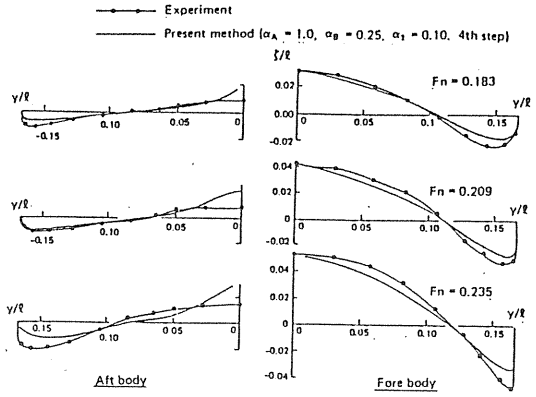

Fig.17 Comparisin of wave profiles for Model B

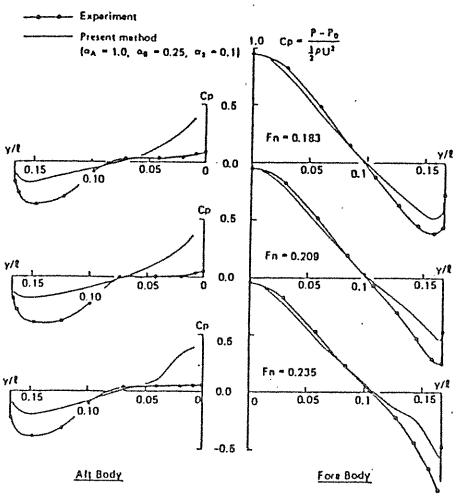

Fig.18 Comparion of pressure distribution for Model B at z/d=-0.3

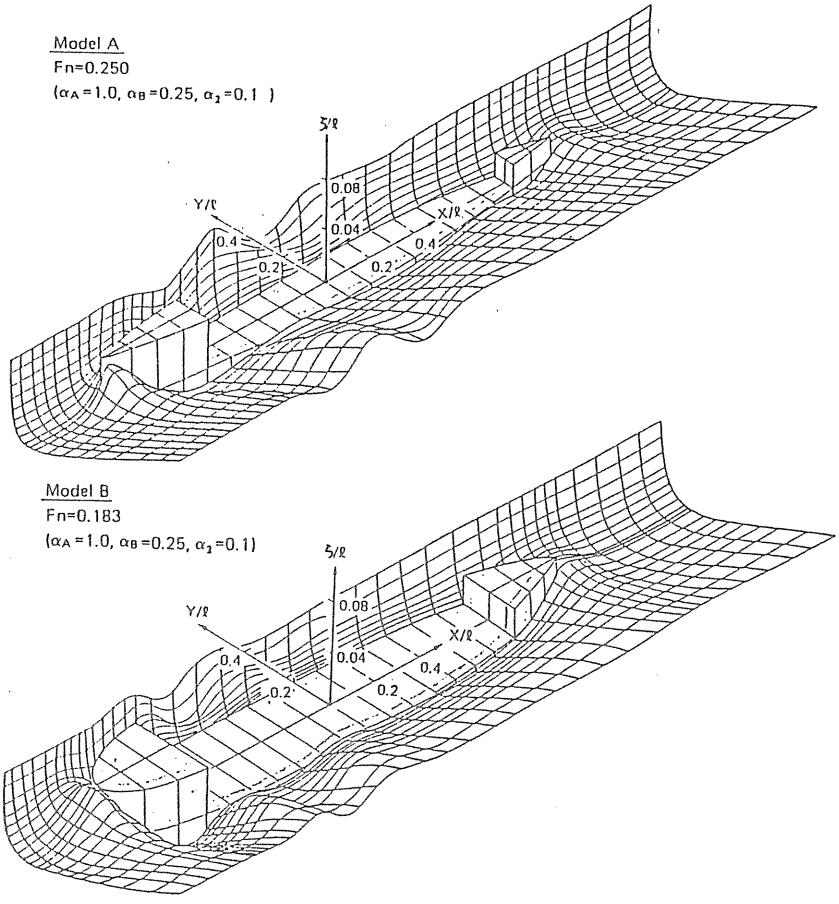

Fig.19 Computed wave patterns around mathematical hulls

Table 1 Mathematical representation of half breadth y for Model B

z \ x	Elliptic form	Parallel part	Parabolic form
	$-\frac{L}{2}\le x\le -\frac{L}{3}$	$-\frac{L}{3}\le x\le \frac{L}{6}$	$\frac{L}{6}\le x\le \frac{L}{2}$
$-\frac{d}{2}\le z\le 0$	$\frac{B}{2}\sqrt{1-\frac{(x+L/3)^2}{(L/6)^2}}$	$\frac{B}{2}$	$\frac{B}{2}\left\{1-\frac{(x-L/6)^2}{(L/3)^2}\right\}$
$-d\le z\le -\frac{d}{2}$	$\frac{B}{2}\sqrt{1-\frac{(x+L/3)^2}{(L/6)^2}-\frac{(z+d/2)^2}{(d/2)^2}}$	$\frac{B}{2}\sqrt{1-\frac{(z+d/2)^2}{(d/2)^2}}$	$\frac{B}{2}\left\{1-\frac{(x-L/6)^2}{(L/3)^2}\right\}\sqrt{1-\frac{(z+d/2)^2}{(d/2)^2}}$

L ; ship length B ; ship breadth d ; draft

The wave resistance is defined by the pressure integral over the hull surface. If the pressure is calculated at each point and is assumed uniform in each panel $\Delta s(i)$, the wave resistance is given by

$$R_w=-\sum_{j=1}^{M_s}\{p(i)-p_0\}\,n_x(i)\,\Delta s(i) \tag{48}$$

Though the fluid velocities are defined in the space below the still water plane z=0, the pressure integral must be taken over the real wetted hull surface under the elevated free surface. Therefore the pressure acting on the hull surface between real free surface and the still water plane should be taken into account. In the present comutation, we assume a linear variation of pressure such as

$$p-p_0=p_w\left(1-\frac{z}{\zeta}\right) \tag{49}$$

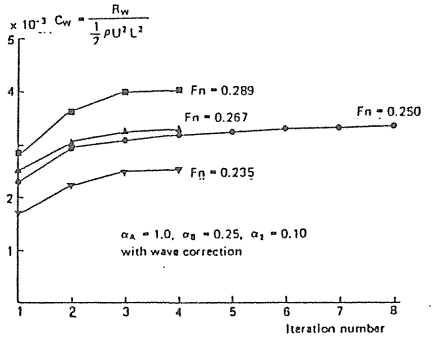

Fig.20 Change of Cw value due to iteration number for Model A

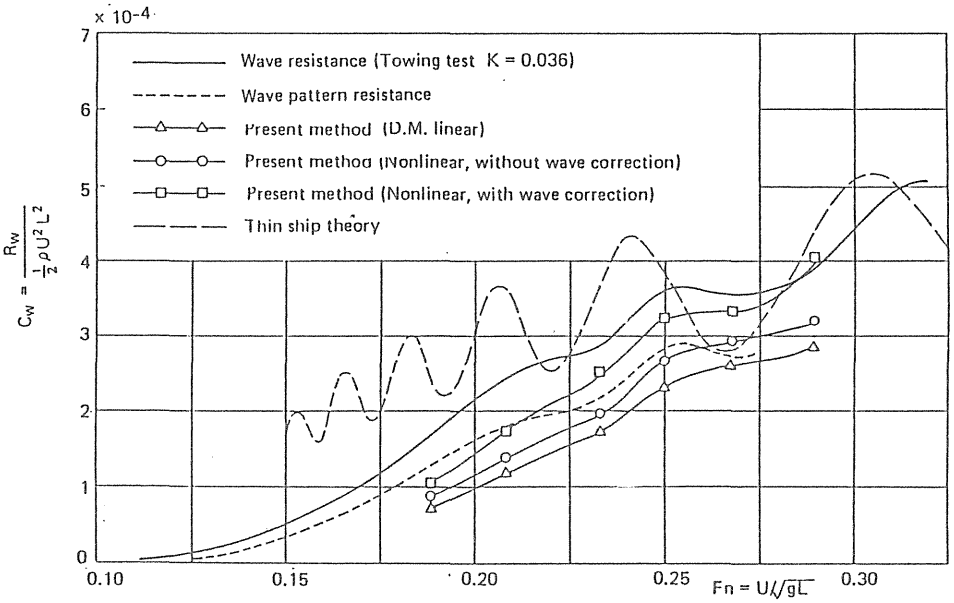

Fig.21 Comparison of wave resistance of Model A

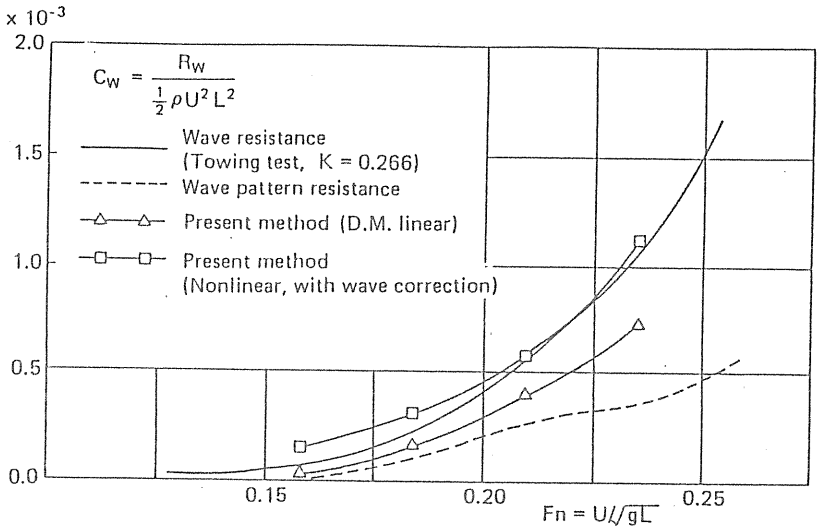

Fig.22 Comparison of wave resistance of Model B

where p_w is the pressure calculated at the still water surface. One can put $p_w=\rho g\zeta(x)$. Then the correction term to be added to equation (48) is

$$\Delta R_w = -\rho g \int_{-l}^{l} \zeta^2(x)\cdot n_x \cdot dx \qquad (50)$$

Fig.20 shows the result of computation of R_w of Model A at each step of iteration. It is observed that the iteration converges at above fourth step. Curves for the wave resistance coefficient as a function of Froude number computed by different methods are compared in Fig.21. In this figure, D.M.Linear means the double model linear solution which is the first approximation of the iteration procedure. The importance of the non-linear effect and that of the wave correction term ΔR_w are clearly observed.

Fig.22 compares the computed and measured wave resistance of Model B. In these figures, the results by the present method have attained a remarkable improvement in agreement with measurement.

8. Concluding remarks

The present work has proposed a method of theoretical computation for the wave pattern and wave resistance by which the non-linearity in the free surface condition is taken into account. The wave profile, pressure distribution on the hull surface and wave resistance of models with simple hull forms are computed and the results are compared with measurement in the towing tank. The conclusion is as follows.

(1) The results of computation by the present method show fairly good agreement with measurements, so that this method has a feasibility as a practical method of computation for arbitrary hull forms.

(2) The adoption of the relaxation factor α_1 and α_2 enables the iteration process to be stable. α_1 has a function of supressing non-linear instability at excessively high wave crest by which the wave breaking is liable to take place.

(3) The computed wave profile, pressure distribution and wave resistance show a plausible agreement with measurement in both fine and full models in general, but some discrepancy is observed in the wave profile and pressure distribution at the stern of full model where the boundary layer separation is likely to take place

(4) The non-linear effect is significant near the bow and stern ends of the hull where the wave crest is much steeper than that predicted by the double-model-linearized approximation.

(5) The wave resistance computed by the present method is considerably higher than that predicted by the double-model-linearized approximation.

Acknowledgements

The numerical work was carried out by using HITAC M-280H computer of the Computer Center of University of Tokyo, through the remote station at Yokohama National University Computer Center. The authors express their thanks to Dr.K.Suzuki and Mr.I.Okada for assistance in the computation.

The experimental work was carried out at the ship model basin of Research Institute of Ishikawajima-Harima Heavy Industries Co.,Ltd. The authors are grateful to Prof.T.Jinnaka, Dr.R.Tasaki, Mr.M.Namimatsu, Mr.T.Yamasaki and Dr.T.Tsutsumi for their useful advice.

This work is partly supported by the Grant-in-Aid for Scientific Research

References;

1. Tsutsumi,T.,Ogiwara,S., On the principal particulars of ship hull form and wave pattern resistance (II), Journ. Soc.Naval Arch. Japan Vol.137 (1975)
2. Wehausen,J.V., An approach to thin ship theory, Int.Seminar on Theoretical Wave Resistance, Ann Arbor (1963)
3. Maruo,H., A note on the higher order theory of thin ships, Bull. Faculty Eng. Yokohama Nat. Univ. Vol.15 (1966)
4. Eggers,K.W.H., Second oder contribution to ship waves and wave resistance, 6th Symp. Naval Hydro. Washington D.C. (1966)
5. Ogilvie,T.F., Wave resistance, the low speed limit. Rep.No.002, Dept. Naval Arch. Marine Eng. Univ. Michigan (1968)
6. Baba,E., Takekuma,K., A study on free surface flow around bow of slowly moving full forms, Journ. Soc. Naval Arch. Japan, Vol.137 (1975)
7. Maruo,H.,Suzuki,K., Wave resistance of a ship of finite beam predicted by the low speed theory, Journ. Soc. Naval Arch. Japan, Vol.142 (1977)
8. Dawson,C.W., A practical computer method for solving ship wave problem, 2nd Int. Conf. Numerical Ship Hydro., Berkeley (1977)
9. Ogiwara,S., A method to predict free surface flow around ship by means of Rankine sources, Journ. Kansai Soc. Naval Arch. Japan, Vol.190 (1983)
10. Chan,R.K.C.,Chan,F.W.K., Numerical solution of transient and steady free surface flow about a ship of general hull shape, 13th Symp. Naval Hydro., Tokyo (1980)
11. Aoki,k., Miyata,H., Masuko,A.,Kajitani,H., A numerical analysis of nonlinear wave generated by ships of arbitrary waterline, Journ. Soc. Naval Arch. Japan, Vol.154 (1983)
12. Ogiwara,S., A numerical method of non-linear solution for steady waves induced by two-dimensional submerged bodies, Journ. Soc. Naval Arch. Japan, Vol.156 (1984)
13. Ogiwara,S.,Maruo,H., A numerical mothed of non-linear solution for steady waves around ships, Journ. Soc. Naval Arch. Japan Vol.157 (1985)

以下の頁は著作権者の許諾を得ていないため、公表できません。

p. 9 ~ p. 21

p. 34 ~ p. 42

p. ~ p.

p. ~ p.

p. ~ p.

Some Discussions on the Free Surface Flow Around the Bow

H. MARUO AND M. IKEHATA

Yokohama National University, Japan

ABSTRACT:

In order to elucidate the free surface phenomena around the ship bow, experiments of simple wedge-shaped models are conducted in the towing tank. It is found that the surface tension has a remarkable effect on the free surface pattern around the model. It is shown that the surface activator compound is very effective in order to remove the effect of the surface tension. Free surface configurations free from the surface tension observed by photographs after application of the surface activator are examined in detail. In order to apply the theoretical analysis to the wave pattern under the effect of the surface tension, the ray theory is effectively employed, and a differential equation which determines the curve of the capillary wave front around the wedge is obtained. The ray theory is applied also to the wave pattern at the bow when the surface tension is eliminated, and it is concluded that the wave configuration changes its characteristics, when the entrance angle exceeds 60 degrees. This fact is clearly proved by the experimental observation. Next the effect of surface tension to the resistance of ship models is examined by means of the application of the surface activator to the resistance test. A considerable difference in the resistance is observed when the surface tension is removed. Therefore the scale effect due to the surface tension should be taken into account in the lower speed range.

1. INTRODUCTION

The free surface flow around the ship bow has drawn attention in naval architects in recent years.[1] Among free surface phenomena, the breaking of waves at the bow is of special importance because of its relevance to the resistance of full-hull-forms. There have been several attempts to elucidate the mechanism of wave-breaking at the bow so far, which propose various kinds of hypothesis. However most of these hypotheses are not likely to be acceptable by the rational basis of hydrodynamics of Newtonian fluid, and some critical comments on the various hypotheses so far proposed have appeared in another literature.[2] In consequence, one can regard that the mechanism of the bow-wave-breaking is not yet unvailed. In order to understand the true situation of the physical phenomena, the detailed observation and accurate measurement of the phenomena are indispensable. Photo 1 gives a typical picture of the wave pattern around the bow of a large tanker(VLCC) in full scale. One can observe several wave crests in front of the stem and the breaking waves take place at these wave crests. However this sort of wave pattern is hardly reproduced in model scale in the towing tank. A typical configuration of free surface around the bow of ship model is shown in Photo 2. Although the hull form of the ship in Photo 1 and that of the model are not identical, the difference between these pictures seems to be a common feature in such a comparison. A preliminary observation in the towing tank has indicated the possibility of existence of a scale effect due to the surface tension in the configuration of the free surface. The free surface disturbane under the effect of surface tension was first described by Scott Russel[3] and Kelvin,[4] and mathematical investigation was given by Rayleigh.[5] Typical wave patterns associated with a point disturbance were shown in Lamb's text.[6] It is possible to take account of the surface tension in the thin ship theory as Webster did.[7] According to these theories, the effect of surface tension may be neglected if the speed of advance is sufficiently greater than the critical velocity of gravity-capillarity waves i.e. 0.23m/sec, because the ratio between the lengths of the gravity wave and the capillary ripples is very great. In order to examine how the surface tension influences the configuration of free surface, a series of experiments with wedge-shaped models have been conducted in the towing tank.[8] It has been found that the application of surface activator compound on the water surface reduces the surface tension to a great extent. The comparison between the free surface pattern when the surface activator compound is applied to the water surface in front of the model and that without such process, for

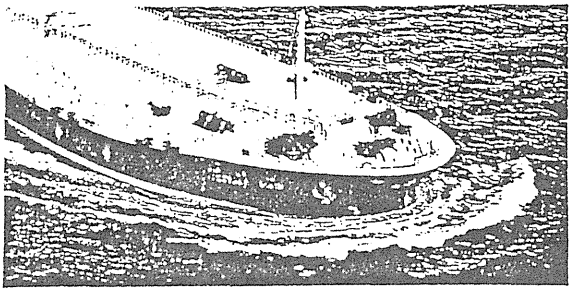

Photo 1 Bow Wave Pattern of a Tanker

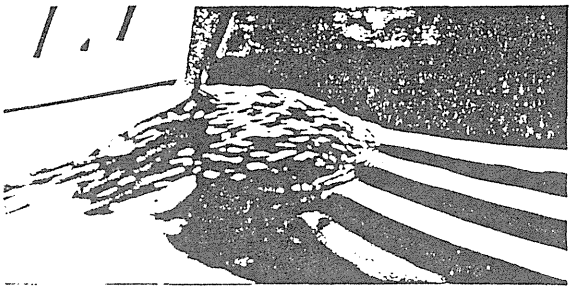

Photo 2 Bow Wave Profile of 5 metre Model of a Bulk Carrier

which the surface tension is intact, indicates that the conclusion of above theories is different from the truth. The difference in free surface pattern in front of the model is significant even if the speed of advance exceeds the critical speed considerably. Specifically, a considerable difference is observed in the wave breaking between two cases.

It is taken for granted in today's practice of ship model test in the towing tank, that Froude's hypothesis is valid, that means the resistance originated from free surface phenomena is a function of Froude number and the change in Reynolds number or Weber number can give only a negligible effect. If the free surface flow around the ship model is subject to the influence of the surface tension to a considerable extent, however, the influence to the model resistance may not be neglected. Since the Weber number for the ship in full scale is extremely great and her resistance is free from the effect of surface tension, the scale effect due to the surface tension seems to be present in the model scale. If this is true, the existing practice of the model-ship correlation method, which is based on the assumption that the resistance coefficient is a function of Reynolds number and Froude number, may need to revise. One of the purpose of the present investigation is to examine how the flow pattern around the model is influenced by the surface tension.

Since the application of the surface activator compound to the free surface almost eliminate the surface tension near the model, the free surface pattern free from the surface tension can be observed. Then one can examine the free surface phenomena free from surface tension, which can be correlated with phenomena in full scale. This process will enable a sound discussion of the mechanism of wave-breaking.

2. OBSERVATION OF THE FREE SURFACE AROUND WEDGE-SHAPED MODELS

It has been found by the preliminary experiment, that the surface activator is very effective to remove the surface tension. For the purpose of comparison of the flow pattern under the effect of surface tension with that free from the surface tension, a solution of surface activator compound is spread on the free surface by a sprayer in front of the model which is towed through the towing tank. Concentration of the compound in the solution is small in order to avoid the pollution of tank water, nevertheless the effect is proved enough to reduce the surface tension to a great extent. Models employed in the experiment are wedges with 230mm breadth and 950mm draft. Entrance angles (1/2 apex angles) of the wedges are 30°, 45°, 60°, 70° and 80°. The models are fixed to the carriage of the towing tank and towed with speed from 0.8m/sec to 1.35m/sec. The free surface is observed by taking pictures from model side and from ahead. In order to reinforce contrast of the picture, a screen board with white and black stripes is placed behind the model. Typical samples of the picture are given in Photo 3-a through Photo 17-b. Stripes on the water surface in the picture are the image of the back screen. Pictures on the left are the case for which the surface activator is not applied while those on the right are the case for which the surface tension is removed by the application of the surface activator. One can observe a remarkable change of the free surface configuration after the process of eliminating surface tension. Photos 3-a, 4-a, 5-a show the case of entrance angle 30° when the surface tension is intact. At lower speed such as 0.8m/sec, there is a curved line of step wave front circumscribing the wedge bow and capillary ripples appear outside the wave front line. Inside this line, there is the silent zone where no wave exists. This type of wave pattern is a characteristic feature of the free surface around the bow at low speed when the surface tension is present. When the speed increases, the wave-breaking takes place at the wave front line above-mentioned (Photo 2-a), and at higher speed, the breaking wave is fully developed until the wedge bow is encircled by a chaotic turbulent zone (Photo 3-a). The free surface after the surface tension is removed by the application of surface activator is shown in Photos 3-b, 4-b, 5-b. The capillary wave front together with ripples disappear and one can observe Kelvin-type diverging wave system starting from the apex of the wedge (Photo 3-b). At slightly higher speed such as 1.0m/sec, a small wave crest appears in front of the bow (Photo 4-b) and as the speed increases, wave-breaking takes place at the position of this wave crest (Photo 5-b). When the speed increases further more, the wave-breaking stretches out on wider area, and the difference between the case under the effect of surface tension and that free from the surface tension

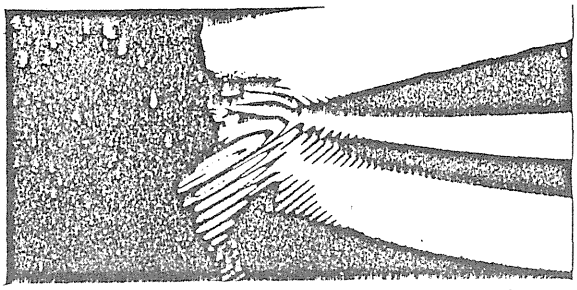

Photo 3-a Wave Pattern under Surface Tension
α = 30°, V = 0.8m/sec

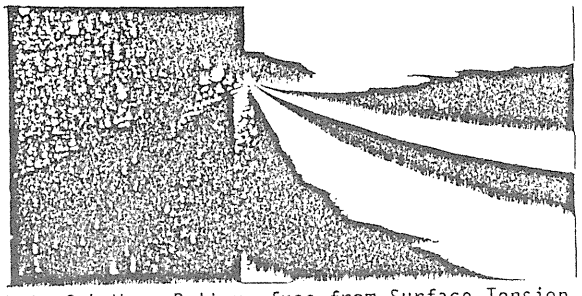

Photo 3-b Wave Pattern free from Surface Tension
α = 30°, V = 0.8m/sec

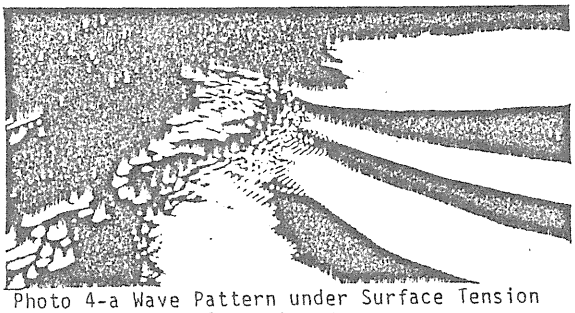

Photo 4-a Wave Pattern under Surface Tension
α = 30°, V = 1.0m/sec

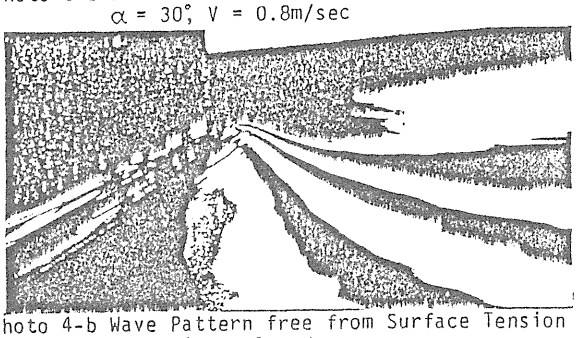

Photo 4-b Wave Pattern free from Surface Tension
α = 30°, V = 1.0m/sec

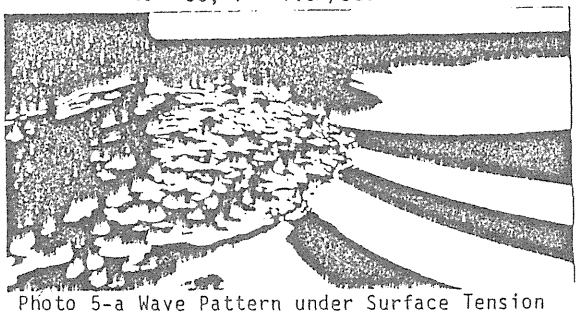

Photo 5-a Wave Pattern under Surface Tension
α = 30°, V = 1.1m/sec

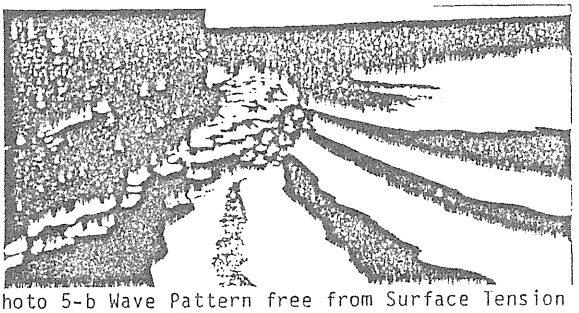

Photo 5-b Wave Pattern free from Surface Tension
α = 30°, V = 1.1m/sec

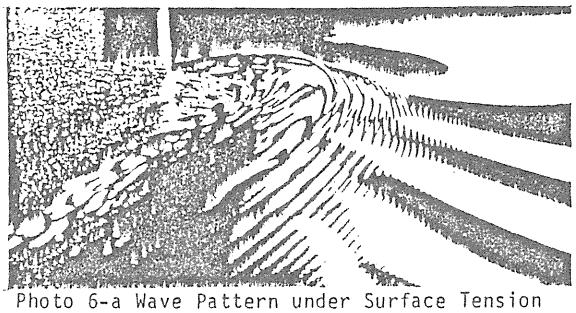

Photo 6-a Wave Pattern under Surface Tension
α =45°, V = 1.1m/sec

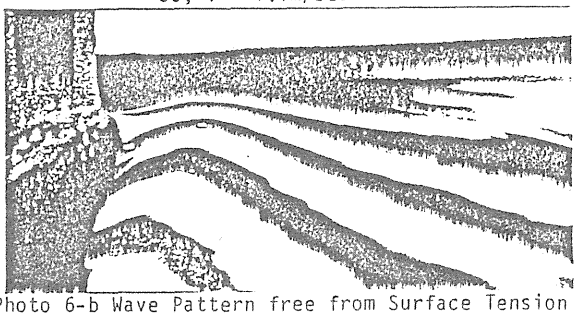

Photo 6-b Wave Pattern free from Surface Tension
α = 45°, V = 1.1m/sec

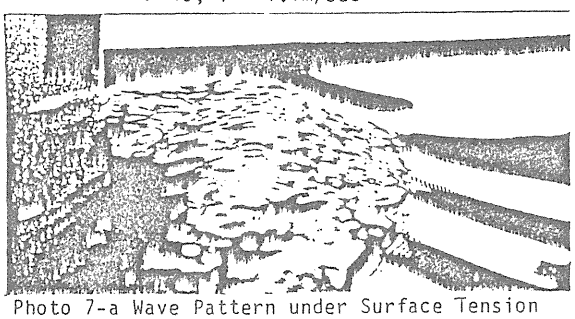

Photo 7-a Wave Pattern under Surface Tension
α = 45°, V = 1.2m/sec

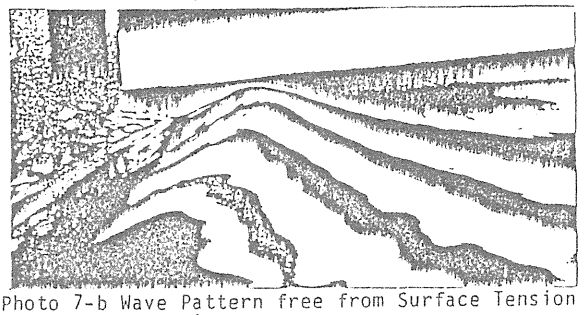

Photo 7-b Wave Pattern free from Surface Tension
α = 45°, V = 1.2m/sec

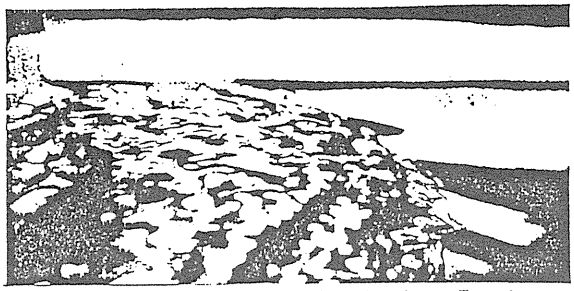

Photo 8-a Wave Pattern under Surface Tension
α = 45°, V = 1.3m/sec

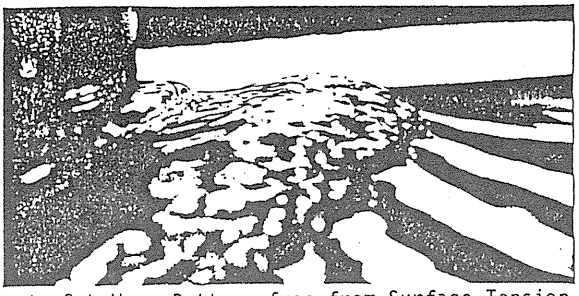

Photo 8-b Wave Pattern free from Surface Tension
α = 45°, V = 1.3m/sec

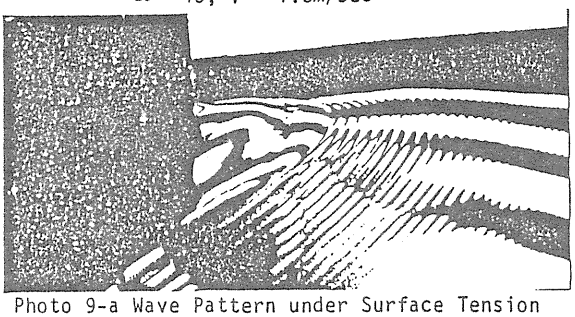

Photo 9-a Wave Pattern under Surface Tension
α = 60°, V = 1.1m/sec

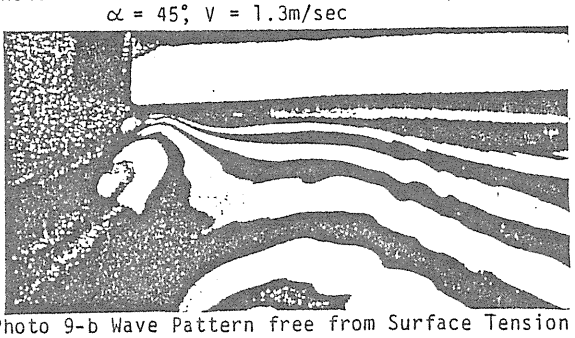

Photo 9-b Wave Pattern free from Surface Tension
α = 60°, V = 1.1m/sec

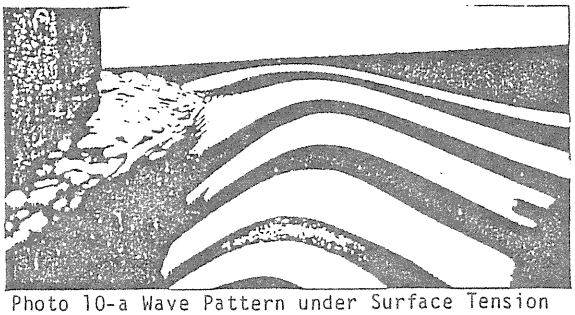

Photo 10-a Wave Pattern under Surface Tension
α = 60°, V = 1.2m/sec

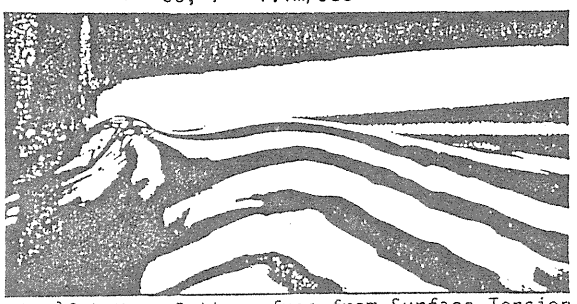

Photo 10-b Wave Pattern free from Surface Tension
α = 60°, V = 1.2m/sec

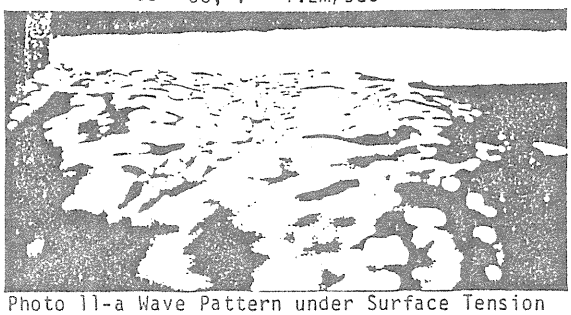

Photo 11-a Wave Pattern under Surface Tension
α = 60°, V = 1.3m/sec

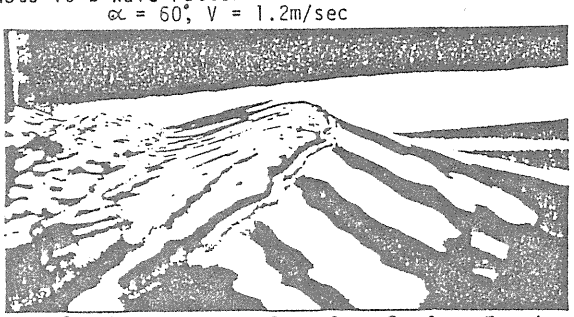

Photo 11-b Wave Pattern free from Surface Tension
α = 60°, V = 1.3m/sec

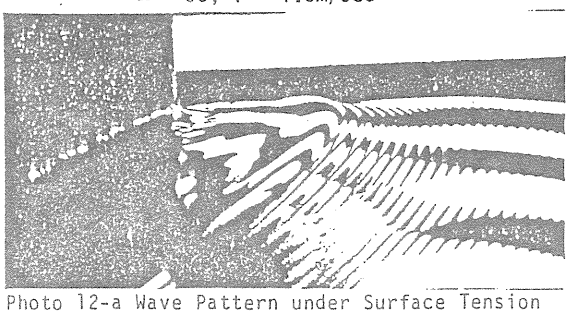

Photo 12-a Wave Pattern under Surface Tension
α = 70°, V = 1.1m/sec

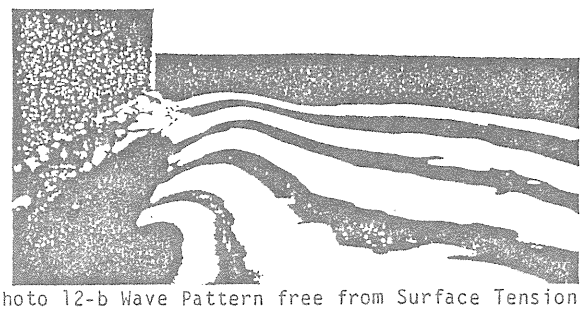

Photo 12-b Wave Pattern free from Surface Tension
α = 70°, V = 1.1m/sec

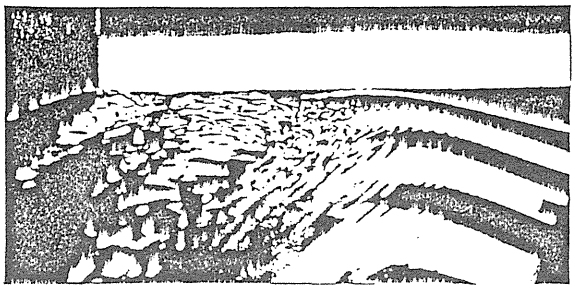

Photo 13-a Wave Pattern under Surface Tension
α = 70°, V = 1.2m/sec

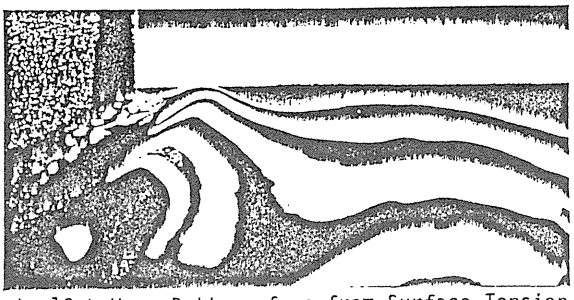

Photo 13-b Wave Pattern free from Surface Tension
α = 70°, V = 1.2m/sec

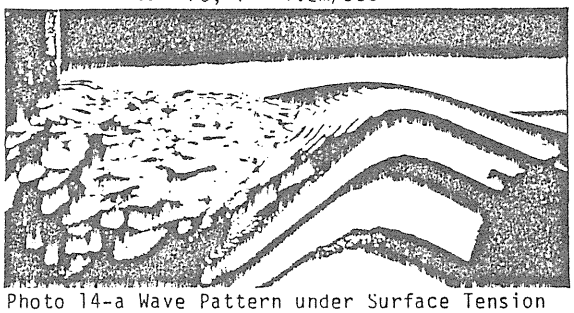

Photo 14-a Wave Pattern under Surface Tension
α = 70°, V = 1.3m/sec

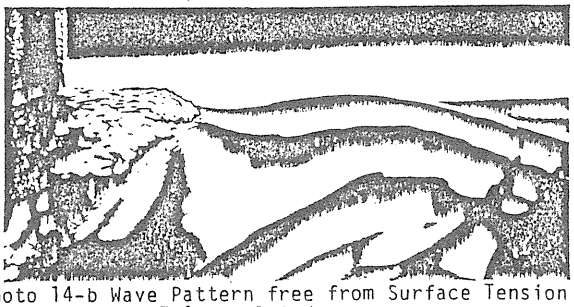

Photo 14-b Wave Pattern free from Surface Tension
α = 70°, V = 1.3m/sec

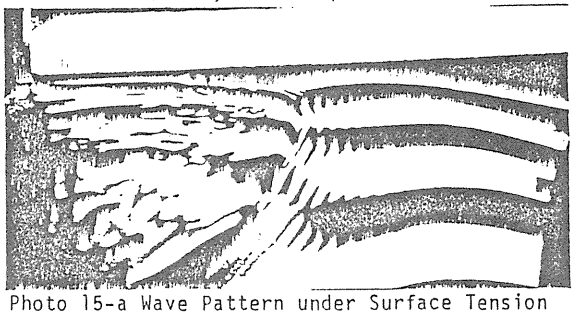

Photo 15-a Wave Pattern under Surface Tension
α = 80°, V = 1.2m/sec

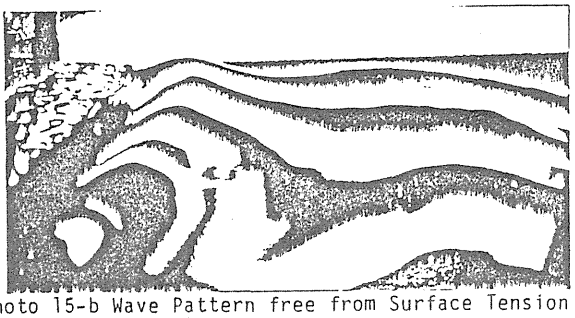

Photo 15-b Wave Pattern free from Surface Tension
α = 80°, V = 1.2m/sec

Photo 16-a Wave Pattern under Surface Tension
α = 80°, V = 1.3m/sec

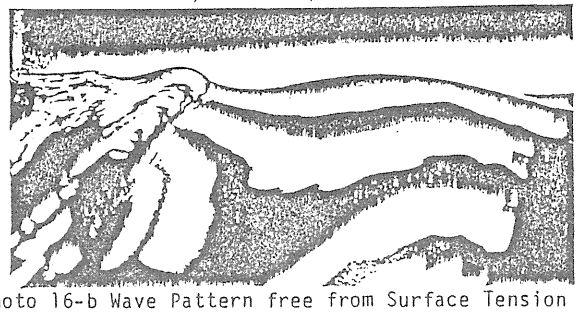

Photo 16-b Wave Pattern free from Surface Tension
α = 80°, V = 1.3m/sec

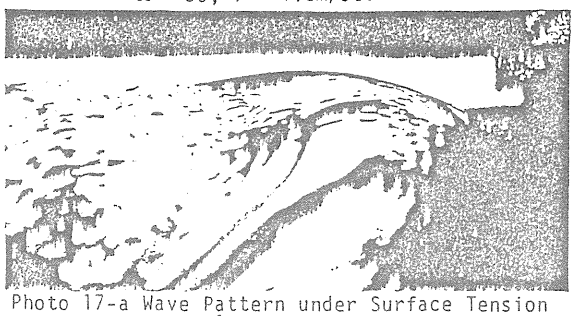

Photo 17-a Wave Pattern under Surface Tension
α = 80°, V = 1.35m/sec

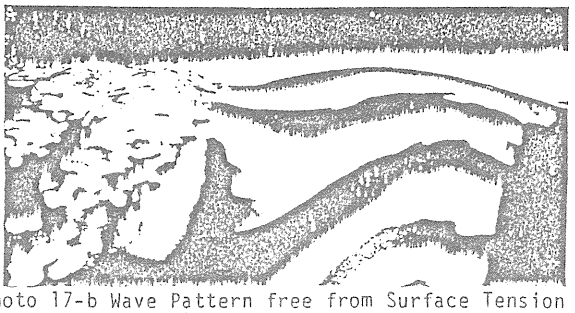

Photo 17-b Wave Pattern free from Surface Tension
α = 80°, V = 1.35m/sec

disappears. At greater angle of entrance such as 45°, the inception of wave-breaking takes place at higher speed irrespective of the existence of surface tension (Photos 7-a,8-b). The wave crest in front of the bow, which appears when the surface tension is eliminated, is more prominent than that of entrance angle 30°(Photo 7-b). The inception of wave-breaking occurs at further higher speed in greater entrance angle such as 60°. The configuration of the free surface under gravity can be examined clearly by the application of the surface activator. As shown in Photo 9-b, a second crest which is more gently-sloping than the first crest just in front of the model appears forward with the entrance angle 60°, and inception of the wave-breaking takes place at these two wave crests (Photo 11-b). The case of entrance angle 70° shows similar phenomena. When the entrance angle increases to 80°, a third wave crest appears further forward (Photo 15-b). The wave-breaking starts at these crests at higher speed.

In any case the wave-breaking takes the type of spilling breaker if the surface tension is not present. Other types such as the plunging or surging type breaking waves have not been observed. There has been an opinion such that the wave-breaking is a phenomenon which is analogous to the hydraulic jump or the free surface shock wave[9] in the shallow water flow, but the present observation indicates that such an analogy may not be warranted. The breaking wave in its initial stage as observed in the pictures looks to be similar to the breaking of ocean waves at critical steepness. The instability at the pointed wave crest may become a trigger of the wave-breaking.

Next the measurement of flow velocity in the center plane forward to the model is carried out by means of a small vane wheel of diameter 3mm. Fig. 1 shows the result for the model with entrance angle 30° at 1.1 m/sec in both cases with and without the process of eliminating surface tension. Fig. 2 shows the result for the same model at 1.2 m/sec. No difference is observed in the velocity distribution between two cases in spite of the difference in the free surface shape. In the part where the wave-breaking is fully developed, a remarkable velocity gradient is observed near the free surface (Fig. 2). This phenomenon is shown more clearly in Fig. 3, which gives the result for entrance angle 45° at 1.3 m/sec. However such a remarkable velocity gradient is not observed if the wave-breaking does not take place even if the wavy elevation appears on the free surface in front of the model as shown in Fig. 4, which gives the result for entrance angle 80° at 1.2 m/sec. Therefore the shear layer, which has been observed by several researchers along the free surface, seems to be associated with the presence of wave-breaking. The opinion,[10] that the free surface shear flow is a consequence of the effect of viscosity on the curved free surface without breaking, is doubtful unless the great curvature of the free surface such as the capillary wave front is present. The formation of necklace vortex may not be analogous to the horse shoe vortex at

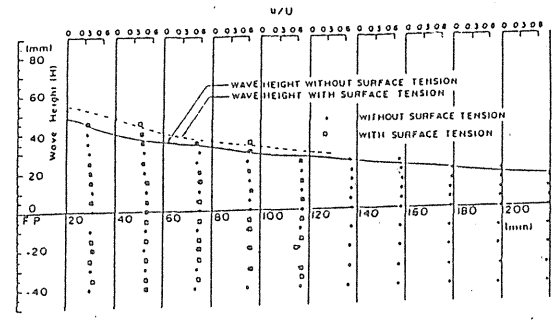

Fig.1 Velocity Distribution α = 30°, V = 1.1m/sec

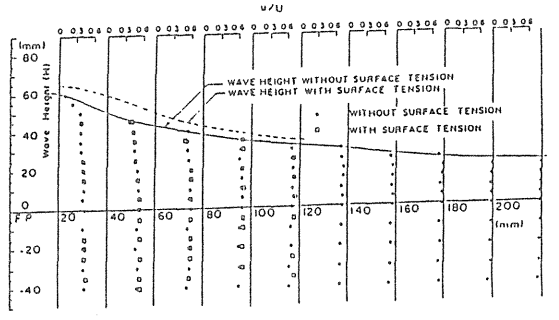

Fig.2 Velocity Distribution α = 30°, V = 1.2m/sec

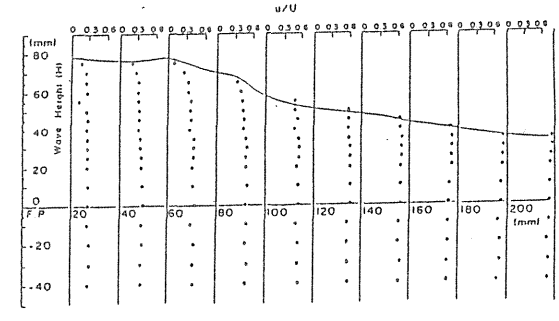

Fig.3 Velocity Distribution α = 45°, V = 1.3m/sec

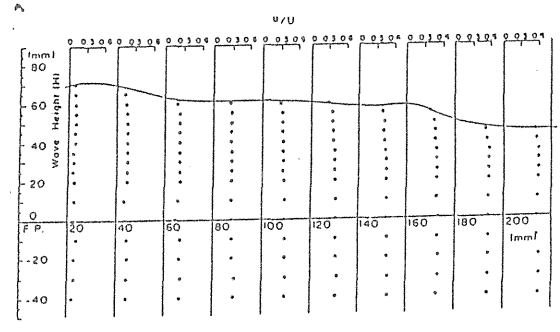

Fig.4 Velocity Distribution α = 80°, V = 1.2m/sec

the base of a body attached to a plane wall,[11] for which the shear flow in the boundary layer plays an important rôle.

3. SOME MATHEMATICAL ANALYSIS

Let us consider the fluid motion around a body fixed in a free surface of a uniform flow of an inviscid incompressible fluid. Take cartesian coordinates x, y, in the undisturbed free surface and the axis of z vertically upwards. The uniform flow is assumed in the direction of positive x. Now we define velocities u_o, v_o, w_o, which are flow velocities when the free surface does not deform as if it were a rigid plane, or they are regarded as velocities around a double body in an unbounded fluid. Because of the free surface elevation, actual flow velocities deviate from u_o, v_o and w_o, and we introduce the velocity potential Φ assuming the irrotational motion in such a way that the velocities are expressed by

$$u = u_o + \Phi_x , \quad v = v_o + \Phi_y , \quad w = w_o + \Phi_z \qquad (1)$$

where subscripts mean partial derivatives. The velocity potential satisfies the Laplace equation

$$\Phi_{xx} + \Phi_{yy} + \Phi_{zz} = 0 \qquad (2)$$

If we assume the speed of advance is low so that the Froude number is sufficiently small, the free surface elevation is very small and the flow deviates only slightly from the double body flow. Therefore the disturbance velocities, grad Φ are much smaller than the base flow velocities of the double body flow. Further we assume that u_o, v_o and w_o are slowly varying while the disturbance velocities vary more rapidly on account of their wavy nature. Introducing the expression (1) in the boundary condition at the free surface under gravity and surface tension, and taking only terms of the lowest order with the consideration of above assumptions, we obtain the linearized free surface condition for Φ such as

$$u_o^2 \Phi_{xx} + 2u_o v_o \Phi_{xy} + v_o^2 \Phi_{yy} + g\Phi_z + \kappa \Phi_{zzz} = \Psi(x,y) \qquad (3)$$

where g is the acceleration of gravity and κ is the kinematical capillarity defined by $\kappa = T/\rho$, T being the surface tension per unit length. This equation is regarded to be satisfied on the plane z=0. The function $\Psi(x,y)$ on the right hand side is the forcing function and determined by the base flow velocities u_o and v_o. Now let us apply the ray theory to the present case. Since the ray theory deals with the propagation of free waves, we employ the homogeneous equation by putting $\Psi(x,y)=0$ as the free surface condition. Assume the infinite depth of water and define the wave potential of the form

$$\Phi = Ae^{iF(x,y,z)} \qquad (4)$$

Let us consider the case of short waves and assume

$$\text{grad } F(x,y,z) = O(\varepsilon^{-1})$$

where ε is a small quantity of the first order. Then the Laplace equation results the relation in the lowest order such as

$$[F_x(x,y,0)]^2 + [F_y(x,y,0)]^2 + [F_z(x,y,0)]^2 = 0 \qquad (5)$$

Because Φ gives the free wave without the exponential decay, $F_x(x,y,0)$ and $F_y(x,y,0)$ are real functions, while $F_z(x,y,0)$ is pure imaginary. Therefore one can define the phase function

$$S(x,y) = F(x,y,0) \qquad (6)$$

Since the fluid motion decays downwards, $iF_z(x,y,0) > 0$. Then one can define the local wave number

$$iF_z(x,y,0) = \sqrt{S_x^2 + S_y^2} = k \qquad (7)$$

Substituting (3) in the homogeneous free surface condition

$$u_o^2 \Phi_{xx} + 2u_o v_o \Phi_{xy} + v_o^2 \Phi_{yy} + g\Phi_z + \kappa \Phi_{zzz} = 0 \qquad (8)$$

and taking terms of the lowest order, we obtain

$$(u_o S_x + v_o S_y)^2 = \sqrt{S_x^2 + S_y^2}\,[g + \kappa(S_x^2 + S_y^2)] \qquad (9)$$

This equation defines the dispersion relation of waves under gravity and capillarity, and becomes the basis of the ray theory. Now we define the wave number vector

$$\text{grad } S(x,y) = \underline{k} \qquad (10)$$

and write $\underline{q}$ for the velocity u_o, v_o on z=0. Then the dispersion relation becomes

$$(\underline{q} \cdot \underline{k})^2 = |\underline{k}|(g + \kappa |\underline{k}|^2) \qquad (11)$$

If the velocity $\underline{q}$ makes an angle Ψ with respect to positive x and the wave number vector makes an angle χ (Fig.5), the following equation is valid.

$$kq^2 \cos^2(\Psi - \chi) = g + \kappa k^2 \qquad (12)$$

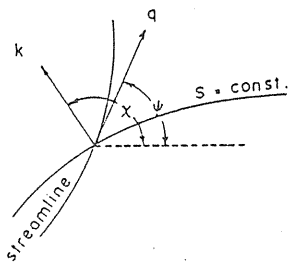

Fig.5 Schematic diagram of the Wave Number Vector

where $q=|\underline{q}|$. The angle χ defines the direction of the ray of elementary waves. Solving the above equation with respect to k, one obtains

$$k = (1/2\kappa)[q^2\cos^2(\psi-\chi) \pm \sqrt{q^4\cos^4(\psi-\chi) - 4g\kappa}] \quad (13)$$

In the case of $q\cos(\psi-\chi)>(4g\kappa)^{1/4}$, there are two wave systems, which have different relations of dispersion. The region where $q\cos(\psi-\chi)<(4g\kappa)^{1/4}$ is the silent zone within which no wave exists. The forward border of the silent zone is the curve of capillary wave front as shown in the pictures of the preceding section. The curve is an iso-phasal line $S(x,y)$=const. along which the following relation is valid,

$$q\cos(\psi-\chi) = (4g\kappa)^{1/4} \quad (14)$$

and the normal to the curve makes an angle with respect to x axis. If we write the equation of the wave front in the form

$$r = f(\theta) \quad (15)$$

making use of cylindrical coordinates $x=r\cos\theta$, $y=r\sin\theta$, the following relation is derived from (14).

$$\cos(\psi-\theta) - \sin(\psi-\theta)f'(\theta)/r = ((4g\kappa)^{1/4}/q)\sqrt{1+\{f'(\theta)/r\}^2} \quad (16)$$

or

$$\frac{f'(\theta)}{f(\theta)} = \frac{\tau^2\cos(\psi-\theta)\sin(\psi-\theta) - \sqrt{\tau^2-1}}{\tau^2\sin^2(\psi-\theta) - 1} \quad (17)$$

where $\tau=q/(4g\kappa)^{1/4}>1$. The solution of this equation determines the curve of the wave front. In order to apply the above equations to the wedge-shaped model, we employ the two dimensional flow illustrated in Fig. 6 as a flow model. A wedge is placed in a uniform stream and is accompanied by the dead flow bounded by two free streamlines along which the pressure is constant. A complete solution for this flow pattern,[12] obtained by the two-dimensional free streamline theory, is expanded around the stagnation point. Then the conjugate complex velocity u_o-iv_o near the apex of the wedge is expressed by

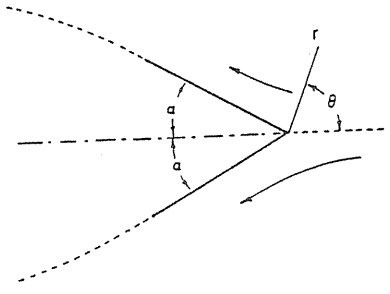

Fig.6 Flow Model around a Wedge

$$u_o - iv_o = -V(ar^{i\theta})^{\alpha/(\pi-\alpha)} \quad (18)$$

where α is the angle of entrance, and a is a coefficient determined by the dimension and the angle of the wedge, given by the equation

$$a = (f/\ell)(1 - \alpha/\pi) \quad (19)$$

where ℓ is the length of each side of the wedge and f is a function of α. In the case of the flow model of Fig. 6, the function f is given by

$$f = 1/4 + \alpha/4\pi + (1/2)(\alpha/\pi)^2[\psi(1-\alpha/2\pi) - \psi(1/2-\alpha/2\pi)] \quad (20)$$

where $\psi(\alpha)$ is the digamma function defined by $\Gamma'(\alpha)/\Gamma(\alpha)$. Then the parameter τ in eq.(17) is expressed by

$$\tau = q/(4g\kappa)^{1/4} = V(ar)^{\alpha/(\pi-\alpha)}(4g\kappa)^{-1/4} \quad (21)$$

The curve of capillary wave front passes the point $x=\ell_c$ on the x axis where $\tau=1$. Therefore we have the relation

$$\ell/\ell_c = f(1-\alpha/\pi)\,\tau_1^{\pi/\alpha-1} \quad (22)$$

where $\tau_1 = V/(4g\kappa)^{1/4}$ (23)

Fig. 7 shows computed results of ℓ/ℓ_c versus τ_1 for several angles of entrance. The curve of

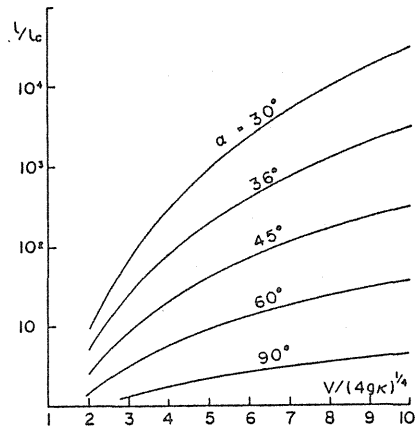

Fig.7 Location of the Capillary Wave Front

capillary wave front is obtained by numerical integration of eq.(17). Fig. 8 shows the result of computation for the cases of the angle of entrance 30°, 45°, and 60°. One may find in these figures that there exists a similarity relation that the curve of wave front for geometrically similar models is determined by the parameter τ_1. Because of the relation

$$\tau_1 = (V/\sqrt{g\ell})((\ell/2)\sqrt{g/\kappa})^{1/2} \quad (24)$$

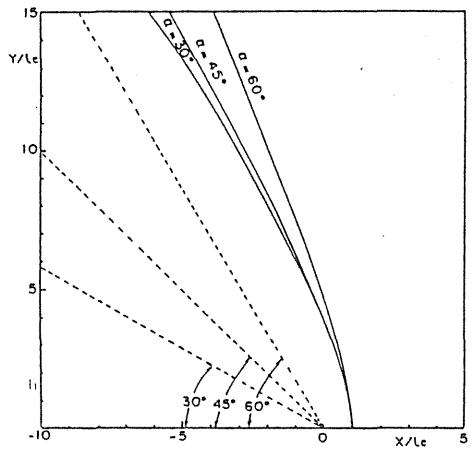

Fig.8 Curves of the Capillary Wave Front

Froude's law is valid under the condition that $\ell\sqrt{g/\kappa}$ is kept constant.

If the surface tension is eliminated, the dispersion relation of wave becomes much simpler such as

$$(u_0 S_x + v_0 S_y)^2 = g\sqrt{S_x^2 + S_y^2} \tag{25}$$

when κ vanishes in eq.(13), the wave number of capillary ripples tends to infinity, while the wave number of gravity waves has the relation

$$k = g/[q\cos(\psi - \chi)]^2 \tag{26}$$

The ray theory in this condition was applied to ship waves first by Keller[13) 14)] and extended investigations have been carried out by Yim[15)] and Tulin.[16)] According to this theory, the wave pattern is obtained from the solution of the differential equation (25). If we transform (25) in the cylindrical coordinates, we obtain

$$(u_r S_r + u_\theta S_\theta)^2 = g\sqrt{S_r^2 + S_\theta^2} \tag{27}$$

where u_r, u_θ are velocity components in r and θ direction respectively, and S_r, S_θ are gradients of S in r and θ direction respectively. Let us consider the elementary wave along the wedge boundary $\theta = \pi - \alpha$. Then we can put $S_\theta = 0$, $u_\theta = 0$, so that the phase function becomes

$$S = g\int_0^r (1/q^2)dr \tag{28}$$

The flow velocity is given by (18) such as

$$q = V(ar)^{\alpha/(\pi-\alpha)} \tag{29}$$

If $\alpha < 60°$, we have the solution

$$S = (g/V^2)a^{-2\alpha/(\pi-\alpha)} r^{(\pi-3\alpha)/(\pi-\alpha)} \tag{30}$$

A similar relation is valid along the center line $\theta = 0$. There exist straight rays passing through the apex of the wedge, and caustics describe the wave pattern which is like the Kelvin-wave system as illustrated in Fig. 9. The cusp line of the diverging wave makes an

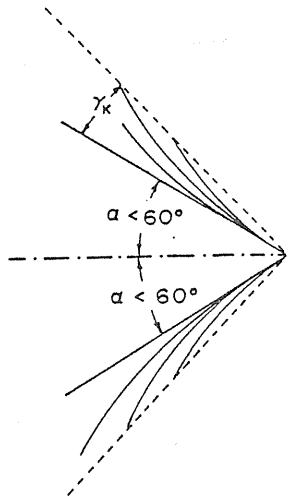

Fig.9 Wave Pattern around the Model $\alpha < 60°$ (schematic)

angle γ with the wedge surface, which is given by

$$\gamma = (1 - \alpha/\pi)\gamma_K$$

where γ_K is the Kelvin angle (19°28′). If $\alpha \geq 60°$, the integral (28) diverges and there is no solution for the phase function around the wedge bow, so that the Kelvin-wave system does not exist, and the disturbance given at the free surface in front of the model does not propagate towards downstream in the form of radiating waves. The bow is encompassed by a turbulent zone as illustrated in Fig. 10 in this case. These phenomena can be observed

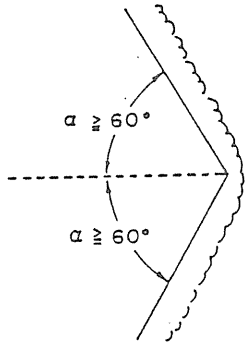

Fig.10 Wave Pattern around the Model $\alpha \geq 60°$ (schematic)

clearly in the experiment by removing the surface tension as shown in Photo 18 for $\alpha < 60°$ and Photos 19, 20 for $\alpha \geq 60°$. The phenomena at the bow of entrance angle not less than 60° may implicate the non-existence of the continuous flow at the bluff bow and relevance to the generation of the necklace vortex around the bow of full hull forms.

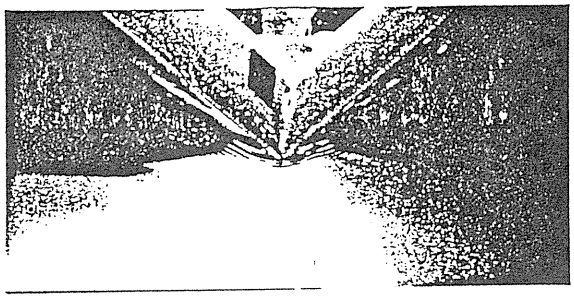

Photo 18 Bow Wave free from Surface Tension
α = 45°, V = 1.1m/sec

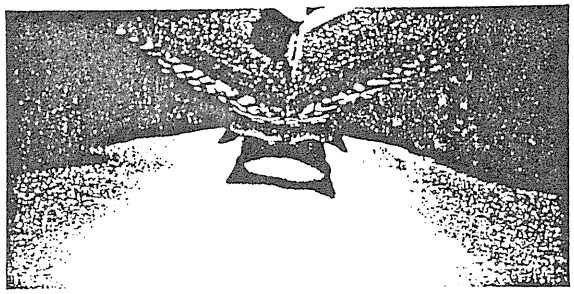

Photo 19 Bow Wave free from Surface Tension
α = 60°, V = 1.1m/sec

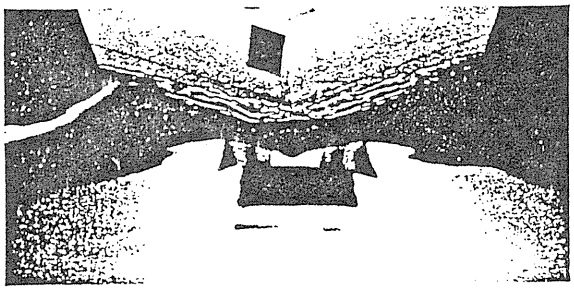

Photo 20 Bow Wave free from Surface Tension
α = 70°, V = 1.1m/sec

4. RESISTANCE OF SHIP MODELS

It has been shown that the free surface configuration around the model is influenced considerably by the surface tension even at moderate speed. Then the effect of surface tension is suspected in the value of the resistance of ship models at the tank test. In order to examine whether the resistance of models is influenced by the surface tension, ship models are towed in the towing tank through water, to which the surface activator compound is applied by spreading on the free surface in front of the models. The resistance measured under this condition is compared with the resistance in unprocessed water in which the effect of surface tension is present. Two models are employed in the experiment. One of them is a 3 metre model of full-hull-form with a cylindrical stem. The other is a 4 metre model of full-hull-form with a wedge-shaped bow of entrance angle 40°. Body plans of the models are shown in Figs. 11, 12. The 3 metre model is tested in two loading conditions,

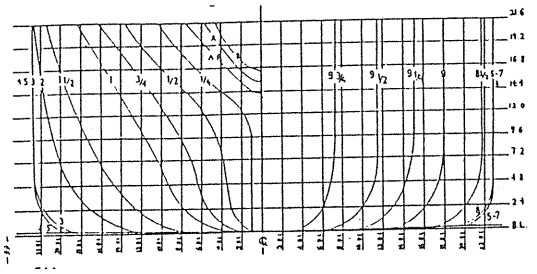

Fig.11 Body Plan of the 3 metre Model

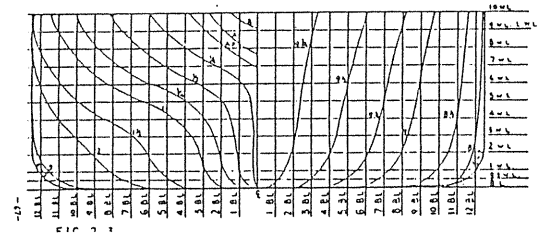

Fig.12 Body Plan of the 4 metre Model

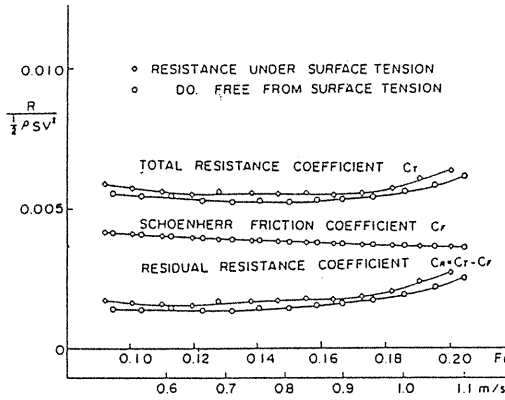

Fig.13 Resistance Curve of the 3 metre Model Full Load Condition

namely full-load and light-load. Fig. 13 shows the result of 3 metre model in full load condition. Consistent difference is observed between the resistance coefficient under the influence of surface tension and that free from surface tension throughout the test speed up to 1.2 m/sec. Photos 21, 22 gives the sample of observation of the free surface, in which we can recognize the effect of surface tension. The turbulent zone around the model which has been explained in the preceding section is observed in Photo 22, in which the surface activator is applied. At higher speed, 0.9 m/sec say, the free surface breaks out even when the surface tension is not present. The difference in the resistance between both cases is possibly due to difference in the area of the wave breaking zone. Fig. 14 shows the resistance coefficients of the same model in light draft. Different from the former case, the effect of surface tension diminishes with increasing speed, and the difference between

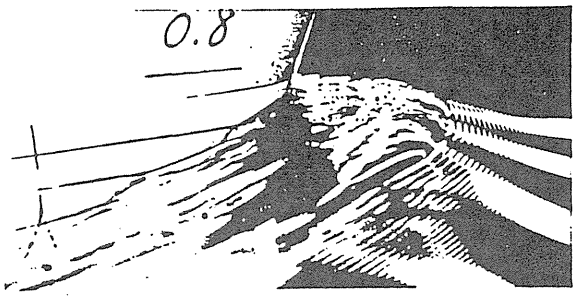

Photo 21 Bow Wave Profile of the 3 metre Model under Surface Tension V = 0.8m/sec

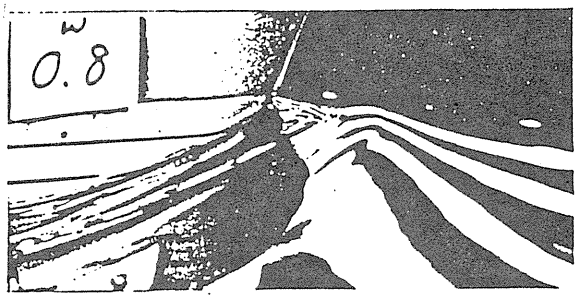

Photo 22 Bow Wave Profile of the 3 metre Model free from Surface Tension V = 0.8m/sec

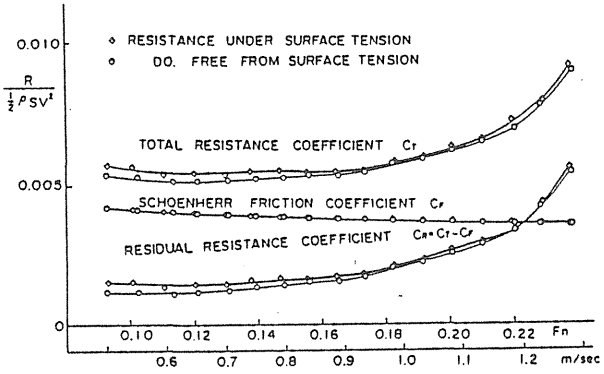

Fig.14 Resistance Curve of the 3 metre Model Light Condition

two curves almost vanish at V=1.0m/sec. The wave breaking takes place at lower speed in the case of light draft than in the case of full load draft. This seems to be one of the reasons of the difference in the effect of surface tension to the resistance curves between the full load draft and light draft. As mentioned in the preceding section, the effect of surface tension is related to the ratio ℓ/ℓ_c given in eq. (22), where f is a function of the entrance angle α. If the draft is finite, f is related to the draft too, in such a way that ℓ/ℓ_c increases as draft decreases. This tendency can be understood by the comparison between a vertical circular cylinder and a sphere with its center on the free surface. Approximate estimates show that

$$r_0/\ell_c \fallingdotseq 2\tau_i \quad \text{for a circular cylinder}$$

$$\fallingdotseq 3\tau_i \quad \text{for a sphere}$$

where r_0 is the radius of the cylinder or the sphere. Therefore the effect of surface tension is less in a shallower draft.

The 4 metre model is tested only at the full load condition. Curves of resistance coefficients are shown in Fig. 15. The diffe-

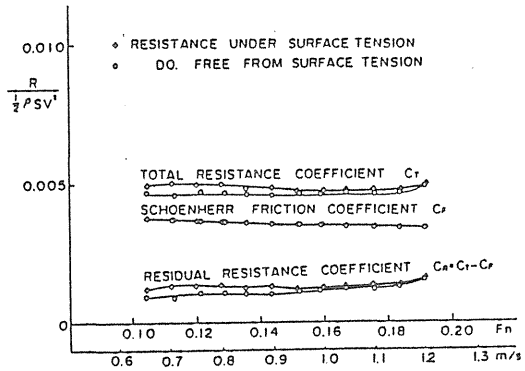

Fig.15 Resistance Curve of the 4 metre Model

rence between the resistance under the effect of surface tension and that free from surface tension decreases as speed increases and vanishes at about 1.15 m/sec, which corresponds to τ_i =5.0. Since the entrance angle of this model is 40°, the corresponding value of ℓ/ℓ_c is about 10^2 according to Fig. 7. Thus the resistance of a ship model is subject to the scale effect due to surface tension, if the tank test is carried out under a certain critical speed. The parameter $V/(4g\kappa)^{1/4}$ may be employed as a criterion for the effect of surface tension. Since Fig. 7 indicates a strong dependence of this effect on the entrance angle, the critical speed is dependent on the entrance angle to a great extent. In the case of the hull form of 4 metre model, the critical speed corresponds to the Froude number greater than 0.18. Therefore the resistance test result is contaminated by the surface tension throughout the whole range of operating speed of full-hull-forms such as oil-tankers and bulk carriers. Even for large models of 6 metre, the critical speed is at the Froude number 0.15, which is still within the important speed range in practice. Another troublesome fact is the difficulty in determination of the form factor for the viscous resistance. If one intends to determine the form factor from the test data at the Froude number 0.10, the error due to the surface tension amounts to more than 20 percent.

5. CONCLUSIONS

Free surface phenomena around the bow are investigated by the use of wedge shaped models. It is found that the free surface configuration is influenced by the surface tension to a great extent. Therefore the free surface phenomena in model scale is not identical with those in full scale, on account of the scale effect due to the surface tension. A particular feature of the existence of surface tension is the capillary wave front which is observed in front

of the model when the wave-breaking does not take place. The wave-breaking starts at the position of this wave front as the speed is increased.

It is found that the surface activator compound is very effective to remove the effect of surface tension. When the surface tension is removed by the application of the surface activator, a remarkable change is observed in the feature of the free surface. Therefore the free surface phenomena in full scale, in which the effect of surface tension is negligible, can be correlated only with model experiments, in which the surface tension is eliminated by the application of the surface activator. The free surface configuration free from the effect of surface tension shows a wave crest or crests in front of the bow. The inception of wave-breaking takes place at these wave crests, showing the spilling type breaking waves, and the hydraulic jump or the free surface shock wave is irrelevant to the wave-breaking at the bow in deep water.

The ray theory is useful to the mathematical analysis of the wave pattern. The curve of the capillary wave front can be calculated by this theory. The wave pattern near the bow of entrance angle less than 60° is like the Kelvin wave system, while such a wave system does not exist when the entrance angle is equal or greater than 60°. In the latter case, the bow is encircled by a chaotic turbulent zone. This phenomenon may be relevant to the generation of the 'necklace vortex' around the bow.

The resistance of ship models is subject to the influence of surface tension. The surface tension results increase in resistance to a considerable extent if the model is towed below a certain critical speed. Then the scale effect due to the surface tension is suspected in the resistance test data at low speed, especially in the case of full-hull-forms with bluff bows. The difference in resistance due to the surface tension vanishes above the critical speed where the breaking waves are fully developed. The critical speed is dependent on the entrance angle and the draft-beam ratio of the model.

ACKNOWLEDGMENTS

The authors wish to express their thanks to Messrs. Z. Takusagawa and I. Okada, staffs of the Marine Hydrodynamic Laboratory, for cooperation. Thanks are also to Messrs. H. Sakamoto, H. Tanikawa, T. Kondo and Y. Morozumi for their participation in the experimental research.

REFERENCES :

1. 17th I.T.T.C. Report of Resistance Committee, Recommendations, Göteborg, 1984
2. Maruo. H., On the breaking of waves at the bow, Symp. on New Developments of Naval Architecture and Ocean Engineering, Shanghai (1983.)
3. Scott Russel, On waves, Brit. Ass. Rep. 1844
4. Thomson, W., Hydrokinetic solutions and observations, Phil. Mag. (4) XVII (1871) 374
5. Reyleigh, Lord, The form of standing waves on the surface of running water, Proc. Lond. Math. Soc. XV (1883) 69
6. Lamb, H., Hydrodynamics, Cambridge Univ. Press. 6th ed. 470
7. Webster, W.C., The effect of surface tension on ship wave resistance, College of Eng. Univ. California, Rep. NA-66-6 (1966)
8. Maruo, H., On the free surface flow around a model bow, Journal Soc. Naval Arch. Japan. 158. (1985) 1-9
9. Inui, T., From bulbous bow to free-surface shock wave-Trends of 20 year's research on ship waves at the Tokyo University Tank, Jour. Ship Res. 25-3 (1981) 147-180
10. Mori, K., Necklace vortex and bow wave around blunt bodies, 15th Symp. Naval Hydro. Hamburg (1985) 303-317
11. Takekuma, K., Eggers, K., Effect of bow shape on free-surface shear flow, 15th Symp. Naval Hydro. Hamburg (1985) 387-405
12. Milne Thomson, Theoretical Hydrodynamics 5th ed. McMilan 347.
13. Keller, J.B., Wave patterns of non-thin or full bodied ships, 10th Symp. Naval Hydro., Cambridge, MA (1974) 543-547
14. Keller, J.B., The ray theory of ship waves and the class of streamlined ships, Jour. Fluid Mech. 91-3 (1979) 465-488
15. Yim, B., A ray theory for nonlinear ship waves and wave resistance, 3rd Internat. Conf. on Numerical Ship Hydro. Paris (1981) 55-70
16. Tulin, M.P., Surface waves from the ray point of view, The Seventh Georg Weinblum Memorial Lecture, Hamburg (1985)

This work is partly supported by the Grant-in-Aid for Scientific Research